Authors' Response:

First of all, thank you to all reviewers for the detailed reviews that help us immensely to improve the manuscript.

1. List of major changes:

- New section about Methodology (section 3) including subsections about 1) field work, trenching, and logging; 2) luminiscene dating; 3) modelling of earthquake occurrence times using OxCal.
- Extensive revision of Section 4: trench descriptions, especially adding subsections about age control to descriptions of trenches SDF1 and SDF3.
- Revision of Section 5, including the OxCal results.
- New section about Completeness of preservation potential of earthquakes in the trenches (section 6.1)
- Extensive revision of section 6.2 (formerly section 6.1) about recurrence rates of earthquakes with M≥6.5
- Addition of explicit description how paleoseismological slip rates were obtained (section 6.3)
- New section about Mmax in the Vienna Basin and the linkage between MF and VBTF (section 6.5)
- Table 1 (formerly table 2) was extended by additional IRSL dating information.
- Table 2 (formerly table 1) was extended by additional information about the single earthquake occurrence times (OxCal results).
- Table 3 was extended by additional information about the combined earthquake occurrence times and respective magnitude estimates.
- Minor changes were applied to Figures 1, 2, 3, 6, 8, 9, 10, 14. New Figures 4 and 12 were added. Figures 5 and 7 were changed to provide more detailed trench logs. Figures 11 and 12 were changed to account the OxCal results.
- Supplementary files containing high-resolution photomosaiques of trenches SDF1 and SDF3 are attached, as well as the OxCal code.

2. Response to RC1 (Ryan Gold):

Major comments

1: Probabilistic framework. This topic has been also brought up by RC2 (Dan Clark). We were not aware that OxCal can also be used for IRSL dating results; we thought that it was mostly used for calibration of radiocarbon ages. Since all the time constraints for our trenches come from IRSL dating, we thought that OxCal was not applicable in this study. But following the suggestion of both reviewers, we managed to transfer our IRSL dating results into OxCal and obtained good results. However, the results are comparable to the results previously shown in the manuscript. We added the resultant occurrence intervals to tables 2 and 3. We also changed Figure 10 (now figure 11) and added Figure 12 showing the recurrence rates for both slip models.

2: Earthquake correlation between sites. Again, this topic was also raised by RC2. We were not aware that the numbering that we used suggests 8 earthquakes in total (when there is evidence for 5-6). What we had in mind was the overall number of possible correlations between trenches and an easy way of reference to each single correlation. Unfortunately, this caused more confusion than the intended clarification. Therefore, we changed the labeling in text, figures and tables in the way suggested by RC1 (E1, E2, E3, E4a, E4b, E5a, E5b, E6a). We also changed the seemingly confusing term “event line” to “slip model”. Regarding the comment on earthquake occurrence times given as ranges vs. as PDFs: The dating constraints along the MF in the Vienna Basin are loose for each single event. The resulting PDFs for earthquakes along the MF are broad distributions with large standard deviations. Therefore, we though that it would be more straight-forward to rather show the time brackets than to construct mean dates with large error bars. However, we added the OxCal results to tables 2 and 3 to provide both types of information.

3: Periodic vs. clustered. Yes, you are right, the uncertainties for the recurrence rates are large. Nevertheless, we wanted to stress out the importance of such possibilities. We did calculate the COV for each slip model and obtained a COV > 1 for the clustered slip model, higher than for the periodic slip model. However, we are hesitant to use it because of the small sample size. Most studies, where COV were applied to distinguish between periodic and aperiodic behavior, had at least 10, or even 25 earthquake occurrence times. In such cases, the COV are more meaningful than in the study here.

4: Characteristic vs. super-cycle. Yes, you are right, we got confused here. The reason why we mentioned it here was because it seems that these faults also are quiet for a long time and then are switched on (maybe triggered by the VBTF). Hence the comparison to the characteristic vs. super-cycle. But in hindsight, we agree that it is better to stick with the discussion about periodic vs. clustered. We changed the introduction in this sense.

5: Unit ages. Yes, we agree. It was hard to find the right place within the paper to describe the dating results. We did not want to present the dating results before the method. By including a methodology section into the manuscript, this problem is solved, and we added the age of the units to the new sections about age control for each trench, where available.

6: Linkage to the Vienna Basin Transfer Fault. We do think that the MF is connected to the VBTF via the common detachment, and we also mention it shortly that in the discussion about the possible activation of the detachment during an earthquake along the MF. However, there is no final/published paleoseismological data yet to link both faults.

7: Geomorphic site/topo profiles. In order to keep the number of figures in check, we thought that Figure 3 would be enough to present the general situation along and below the trench sites. But as suggested by all three reviewers, we have added a close-up geomorphic map for both trenches as well as pictures from the trench sites and hope that this gives a better understanding for the reader (Figure 4).

Moderate/general comments:

1: Event lines. We changed the seemingly confusing term “event line” to “slip model”.

2: Subjective word choice. Thanks to your detailed supplementary commentary, we changed/deleted the respective terms.

3: Mmax for the Vienna Basin. You are right, a combined rupture would lead to a larger earthquake magnitude. And we also think that this a very important part to keep in mind. But since we focused in this paper on data for the MF and the impact of this fault to the seismic hazard, we thought that the scenario of a combined rupture of the VBTF and the MF might be beyond the scope of this manuscript. There is a study by Hinsch & Decker (2011) presenting different rupture scenarios along the VBTF. The resultant Mmax are in the order of 5.9-6.8 for different segments of the VBTF. So, therefore, a possible combined rupture of the VBTF and the MF would include several parameters and additional options that is better addressed in a manuscript by its own. To address the issue about Mmax that has been brought up also by the other reviewers, we added a section (section 6.5).

4: Luminescence dating. Following the suggestion, we have reduced the chapter about dating and placed it into the methodology part (see also response to major comment 5 on unit ages above and methodology section below).

5: Uncertainties. We added the information in the tables and in the text and explicitly stated in the methodology section that the luminescene dating results are given with 1σ uncertainties (see below).

6: Methods section. Thank you for the suggestion. We restructured the manuscript and added a methodology section including the photomosaic generation, logging, sampling and dating, and details of the OxCal calculations (section 3).

7: Haiti earthquake. Sorry for the typo. As far as I remember the discussion, you were right that the fault that generated the earthquake was already mapped, but was assumed to be not the active/relevant fault strand within the fault system. The then used seismic hazard map of GSHAP (Giardini et al., 1999) shows a much lower exceedance probability for the region around Port-au-Prince than seismic hazard maps after the earthquake (e.g. Frankel et al., USGS Open-File Report 2011). We changed the text to “not considered in seismic hazard analysis” in order to avoid confusion.

2001

OAS Caribbean Disaster Management Project, map similar to Global Seismic Hazard Assessment Program (GSHAP) 1999.

Based on recent seismicity

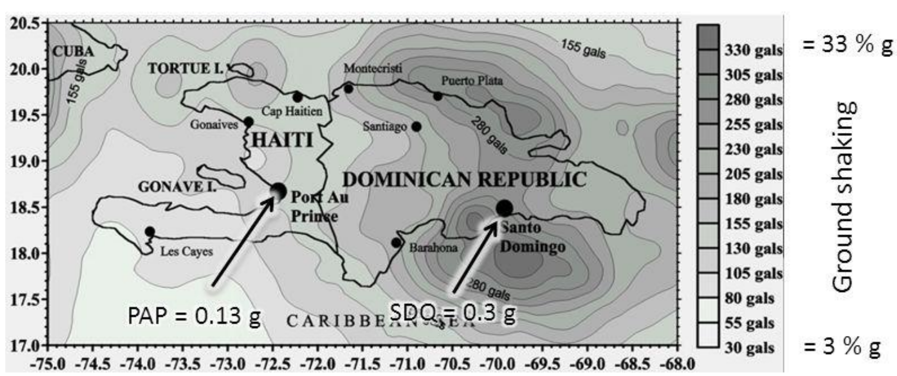

http://www.oas.org/CDMP/document/seismap/

2010

Frankel, A.et al., Documentation for Initial Seismic Hazard Maps for Haiti, USGS Open-File Report 2010.

Includes GPS and some fault information.

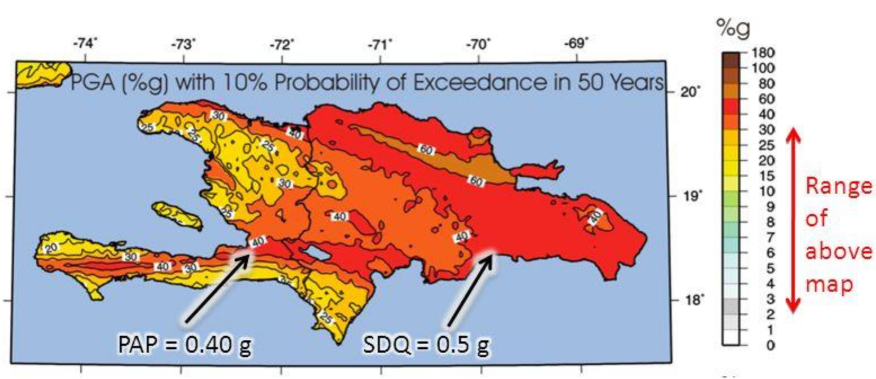

Table 1 and Table 2: We added the additional information to avoid confusion.

Table 3: We changed the numbering of events to make clear that they are only different correlation scenarios. We added also the obtained occurrence interval for each earthquake.

Figures: We made the changes to the figures as suggested by all reviewers, added the uninterpreted photo mosaics to the supplementary, added also a figure of the geomorphic situation/landscape around the trenches, and rearranged Figure 10 (now Figure 11) and added Figure 12 using the OxCal results.

Additional annotated PDF: Thank you for taking the time to annotate the PDF, we changed the manuscript accordingly.

3. Response to RC2 (Dan Clark):

First of all, thanks for the review and the interesting questions that have been mentioned within the review. They definitively will inspire further studies and publications. However, at the moment, trying to answer them would be mostly speculation, because the MF is only the second fault in the Vienna Basin that has been investigated with paleoseismological methods. The other studied fault is a much smaller fault on the western margin of the Gaenserndorf terrace, where there was no clear exposure of the fault within the trench (Weissl et al., 2017). Even though there is information about the long-term Quaternary displacement along most of the faults from boreholes (Decker et al., 2005), detailed information about paleoseismic events along the faults is not (yet) available. Paleoseismological investigations at the VBTF are, at the moment, not finished. Therefore, more work must be carried out before we can address these questions. Hence, we think addressing those questions is beyond the scope of this paper and the data presented here.

Probabilistic framework. This topic has been also brought up by RC1 (Ryan Gold). We were not aware that OxCal can also be used for IRSL dating results; we thought that it was mostly used for calibration of radiocarbon ages. Since all the time constraints for our trenches come from IRSL dating, we thought that OxCal was not applicable in this study. But following the suggestion of both reviewers, we managed to transfer our IRSL dating results into OxCal and obtained good results. However, the results are comparable to the results previously shown in the manuscript. We added the resultant occurrence intervals to tables 2 and 3.

Linkage to the Vienna Basin Transfer Fault. We do think that the MF is connected to the VBTF via the common detachment, and we also mention it shortly that in the discussion about the possible activation of the detachment during an earthquake along the MF. However, there is no ready to be published paleoseismological data yet to link both faults. See also comment to RC1 and RC4. We added a section about the Mmax in the Vienna Basin, where we also discussed this (section 6.5).

General comments:

Labeling of the units. We followed your suggestion and labeled the colluvial units. In addition, due to the comments also provided by the other reviewers, we changed the figures for better understanding of the units and the position of the detailed figures in the trench logs.

Combination of age data between trenches. Due to the recalculation of the occurrence times in OxCal, we have rewritten the section and changed Figure 10 (now Figure 11) accordingly. See also respective comment to RC1. We did calculate the COV for each slip model and obtained higher COV for the clustered slip model than for the periodic slip model. However, we are hesitant to use it because of the small sample size. Most studies, where COV were applied to distinguish between periodic and aperiodic behavior, had at least 10, or even 25 earthquake occurrence times. In such cases, the COV are more meaningful than in the study here.

A larger area than only the MF by rupture of the VBTF and MF. You are right, a combined rupture would lead to a larger earthquake magnitude. And we also think that this a very important part to keep in mind. But since we focused in this paper on data for the MF and the impact of this fault to the seismic hazard, we thought that the scenario of a combined rupture of the VBTF and the MF might be beyond the scope of this manuscript. See also comment to RC1. We added section 6.5 to address this question.

Periodic/aperiodic vs. characteristic/supercycle. Yes, you are right, we got confused here. The reason why we mentioned it here was because it seems that these faults also are quiet for a long time and then are switched on (maybe triggered by the VBTF). Hence the comparison to the characteristic/super-cycle. We changed the introduction in this sense. See also comment to RC1.

Creep. Prior to our study, the MF was suggested to creep aseismically. However, we did not find any evidence for creep in the trenches. See also comment below and comment to RC4.

The **lack of a geomorphic site sketch/map** has also been mentioned by the other reviewers. We included the relevant figure as well as the topographic profile and the landscape picture as suggested and added the names of the towns (see Figure 4). See respective responses to RC1 and RC4.

Far field displacement. Separation of red horizon is due to the sedimentation on pre-existing topography. Besides this, the total topographic step is about 17 m (as visible in Figure 3), but in the trenches, there is no sign for afterslip or interseismic creep.

Threshold for surface rupture in this area and their discoverability. We added a section about the completeness and preservation of earthquake records to discuss this in greater detail (section 6.1).

Mmax as minimum Mmax. Yes, you are right. Of course, this is the Mmax that at least should be considered, based on the data presented here. If interaction between faults and rupture of several segments is considered, the Mmax for the Vienna Basin would be definitively increase. We added a section about Mmax to discuss this in greater detail (section 6.5). See also respective comment to RC1.

Figures: We went through the figures with the annotations in mind, removed all inconsistencies, added and explained labels, where missing, changed Figure 10 (now Figure 11) to add the OxCal results. We finally added the uninterpreted photomosaiques to the supplementary.

4. Responses to RC4 (Maria Ortuño):

First of all, thank you for the detailed review and the suggestions. It was an interesting process to digest the points raised by you, but it helped to address some topics (e.g., gelifluction process, colluvial wedge formation) that we have overlooked to explain previously. In addition, your comments helped immensely to erase any inconsistencies from the figures and to improve them for easier understanding.

Description of wedges and their generation rather by gelifluction processes then by tectonic processes:

During logging and interpreting the trench exposures, we have been very aware of the difficulties to distinguish between gelifluction and tectonic processes, especially because both processes may interfere during periglacial climatic conditions in the Vienna Basin. We have considered this for all the colluvial wedges that they were of non-tectonic origin, but all wedges are either bound by faults or cover faults. In trench SDF1, most of the colluvial wedges are covering tension cracks that are filled with similar material, but showing less overall orientation. The combination of both, the chaotically filled tension cracks together with the colluvial on top of them indicated their tectonic origin for us. Nevertheless, you are right, the process of transporting material from the footwall to the hanging wall might have partly been gelifluction.

The implications to seismic hazard:

1: Periodic vs. clustered behavior: We thought that we have discussed the implication that in the case of clustered earthquakes, the intervals between the clusters should be taken instead of the average recurrence intervals between single earthquakes. We also talked about and calculated the time interval between both clusters to between 32 and 41 ka in section 6.1. (now section 6.2). But you are right, we agree that this an important message and we have stressed this out in greater detail in the conclusions. Due to the comments of the other reviewers, we have rewritten section 6.1 (now section 6.2) and highlighted the differences between periodic and clustered earthquakes. See also comments to RC1 and RC2.

2: Primary vs secondary ruptures: This is definitively a noteworthy topic for discussion that we did not yet discussed in detail. So, thank you for mentioning the topic. This topic is twofold: First, if there are more fault branches reaching the surface during an earthquake apart from the main fault zone exposed in the trenches. We can exclude that on the observations made in the pipeline trench (WAG) that crosses almost the entire area from E to W and proofs that faulting is only observed within the 1-2 m wide zones, just as in the paleoseismological trenches. The trenches were also about 40 long, but there was no additional faulting observed. Second, the observed surface rupture is secondary faulting to earthquakes along the VBTF, which in turn would be a much larger earthquake than just the rupture along the MF. We added a section about Mmax in the Vienna Basin, where we also mentioned a possible secondary rupture along the MF (section 6.5). This was also mentioned by the other reviewers and we answered it further below.

3: Ice loading. We did not discuss this because of the reasons listed below. For the Scandinavian ice shield, the effect would be quite low and would only accounting for the youngest (and smallest) earthquake (around 14 ka). The Alpine ice shield was too small to contribute to a significant loading and the Vienna Basin by itself was not glaciated during the Quaternary. However, normally, this effect is mostly seen for reverse faults and not for normal faults (like the MF).

Paleoseismological data:

1: More detailed geomorphic map. This has been also mentioned by the other reviewers. As mentioned before, we thought Figure 3 would be enough to show the surrounding of the trenches. However, we do see your point and have added figure of the geomorphic/geological situation around the trenches (Figure 4).

2: Picture of the landscape. We added such a pictures to the figure mentioned above (Figure 4).

3. Subunits in logs, location of deformed units, and references in the text. We changed the trench logs following your suggestions and checked the text to include more references to the figures (check Figures 5 and 7). We added the uninterpreted photo mosaics to the supplementary.

4. Event horizons. We did not include event horizons in the trench logs because for most of the faulting events, the event horizon can be only seen in the hanging wall. Therefore, we followed rather the suggestions of RC2 to label the colluvial layers that indicate deposition close after the earthquakes. We hope that marking the colluvial layers in the trench logs help to identify the single earthquakes.

5. Structure of trench log description. Rereading this section, we know that the section description for trench SDF1 and SDF3 look differently. We changed the text and included the colluvial layers in the stratigraphic description of SDF3.

6. Deformation bands. Deformation bands by themselves are defined as small-scale faults with no visible displacement or with displacement in the range of mm. So, the term is used here correctly, because we want to describe exactly those small lines especially visible in sand layers because of their reduced compaction. Maybe there is a misunderstanding, but the deformation bands are not dipping necessarily parallel to the fault zone (they do so in trench SDF1), but are outside the narrow fault zone. We checked the text to avoid any misuse.

7. Description of earthquakes in WAG. We do recognize that this section is too short, especially regarding the event description. We added a more detailed description for the evidence exposed there. However, since this was a construction pit with limited access, exposure and description is rather thin compared to the trenches SDF1 and SDF3.

Different material in hanging and footwall. Yes, we do think that the fault acted as physical barrier for deposition of the fine-grained sediments in the hanging wall, that we interprete mostly as sediments that have been deposited by the River Danube during flooding events. We briefly addressed that in the trench description, but also added that to the interpretation section of the trenches to make it clearer.

Dating results. As suggested by RC1, we moved the dating description to the newly added methodology section (section 3). We added also a subsection about age control to the trench descriptions. This should also solve this problem addressed here.

Paleoseismological discussion:

1) Event definition. We do see your point of firstly addressing the bracketing units and changed the relevant sections accordingly. We though that this is clearly seen the trench logs, but of course you are right, it is better to explicitly mention it in the text. So, we changed it and added an "Age control" section to the trench descriptions (section 4). Figure 10 (now Figure 11) has been changed to accommodate the OxCal results as suggested by RC1 and RC2.

2) Mmax. We are a little confused by this comment, so I hope that I address it correctly. In the first section 6.3 (sorry for the typo, now 6.4), we do compare the maximum magnitude from the trenches (derived from inferred surface displacement, 6.8 ± 0.1) to the magnitudes derived from the fault length and from the fault area (6.7 ± 0.3). In order to make it clearer for the reader, we added the resulting magnitude to table 3 and referenced it to this section. However, we do prefer to keep the discussion of each earthquake together. Regarding the use of Wells & Coppersmith (1994): We are aware that the use of this correlations is slightly outdated, but on the other hand, most paleoseismologists in Central Europe have used those equations to estimate the magnitudes. Therefore, we decided to use the same equations for better comparison of the events within Central Europe. Nevertheless, for further recalculations, we added the observed displacements that are used for the calculations (table 2).

3: Periodic vs. clustered behavior. See comments below and above.

4: Linkage to the Vienna Basin Transfer Fault. The other reviewers also raised this question. We do think that the MF is connected to the VBTF via the common detachment, and we also mention it shortly that in the discussion about the possible activation of the detachment during an earthquake along the MF. The topic about primary vs. secondary faulting is very interesting one, and a topic to explore in further studies. However, at the moment, the data presented here strongly suggest the inclusion of the MF as primary earthquake source. We cannot, and don't want to, exclude the possibility that the MF is also activated as secondary source for the VBTF. But since we focused in this paper on data for the MF and the impact of this fault to the seismic hazard, we thought that the scenario of a combined rupture of the VBTF and the MF might be beyond the scope of this manuscript. We added a section about the Mmax and discussed here also the linkage between both faults (section 6.5). See also comment to RC1 and RC2.

Comments in the supplementary:

Abstract:

1: conservation potential of earthquake surface ruptures smaller than 6.5. Yes, we think that we have shown and discussed that at the beginning of section 6.1, in respect to the exclusion of E1 from the recurrence interval calculation. This might be different in areas with finer sedimentary record, but here in the setting of our trenches, we think this is valid conclusion to draw. We rewrote the section in order to state this more clearly (see the new section 6.1).

2: Magnitude estimates. This is discussed in the second section 6.3 (now 6.4, sorry again for the typo). The largest inferred surface ruptures in both trenches are up to 2 m, suggesting an earthquake around magnitude M~7.0. The magnitude can also derived from the rupture area of an earthquake, not only the length. The fault area of the MF without the detachment area would be a little too small to generate an earthquake of such size. Including the detachment area, the resultant magnitude would fit better to the magnitude observed from the surface displacement. We know that this is not a fact, but we think that it is a possible valid interpretation.

Geological setting:

Historical earthquakes. In principal, you are right. The uncertainties are too large to exclude the activation of the splay faults via small historical earthquakes, especially since earthquakes seem to cluster close to the areas where the splay faults connect with the VBTF. So, it would be possible that there have been small earthquakes at the southern tips of the splay faults. However, north of the River Danube, close to and in Vienna, where the splay faults have their largest throw (shown in industrial seismic data), there is a significant lack of earthquakes, and no historical earthquakes. The few earthquakes there are all instrumental recordings and not larger than ML=3.0. We changed the sentence to avoid further confusion.

MF as creeping fault vs. small earthquakes. Thank you for the comment. We did not realize this paradox and changed the manuscript accordingly.

Paleoseismologically characterized faults: There are none so far, except the Aderklaa-Bockfliess fault, addressed in Weissl et al. (2017). The trenching there did not exposed the fault. The offset of the Quaternary was inferred from geoelectrical data. We stated this more clearly in section 2.

Trenching results:

SDF1. We took your suggestions (also see below) and have rewritten the trench description by using a simpler structure and referencing to the figures, where applicable. See also general comments on paleoseismological data above.

Gelifluction vs. colluvial wedge. Thank you for raising this question here, because the differentiation between gelifluction and tectonic processes is a task that we have been challenged with several times. Interestingly, we did not find evidence for gelifluction in trench SDF1. The colors are post-deposition. However, in trench SDF3 and in another trench in a similar setting (which is not ready to be published yet), we have seen colluvial wegdes that have been affected by gelifluction. These look very different from the wedges in SDF1. We did also not find overturned faults as are typical for fault zones affected by gelifluction. As far as we are aware of, colluvial wegdes can be also formed by (episodic) erosion from the foot wall towards the hanging wall. And this what we think happened here. This would also lead to a layered wedge, but bound at least partly by the fault, which is exactly what we have seen in these trenches here. The initial, more chaotic layering is observed in the underlying tension cracks. We have rewritten the trench description. We hope that with the improved version of the manuscript, the evidence for tectonic origin of the colluvial wedges is better presented.

Tension cracks / filled fissures. We homogenized the terms. The infill consists of the same material as the overlying wedge, but with less oriented. This is one of the reasons why we favor the interpretation of colluvial wedges instead of gelifluction.

Section 3.1.1. According to your earlier comments, we changed this section to provide more information about the bracketing units. However, there are 4 colluvial wedges associated with chaotically filled tension cracks (A2-A5) plus the displacement caused by the youngest earthquake (A1). That are 5 earthquakes. I think there is a misunderstanding, because we state the 4 colluvial wedges are evidence for 4 earthquakes, and then the displacement of the youngest colluvial wedge caused by another earthquake. We changed the wording to avoid further misunderstandings.

Section 3.2.1. Yes, that is the observation that we wanted to describe. We changed the wording to avoid any confusion. We included the fault numbers into the log figure.

WAG trench. As mentioned above, we do recognize that this section is short, especially regarding the event description. This outcrop being a construction pit with limited access, exposure and description is rather thin compared to the trenches SDF1 and SDF3. However, we added a more detailed description for the evidence exposed there. We better stress out the most important observation which is that the fault displaces the loess, reaches the surface, and cuts off the terrace (now Fig. 10A). At the beginning, we were confused what you mean with folding, but then we understand how you came to the conclusion, but folding was not observed there. We hope that with the new description and the improved figures, the situation is better to understand for outsiders.

Luminescence data. As already mentioned above, we followed the suggestions of RC1 and added a section about methodology and moved the description of the dating technique and protocol. We added the uncertainties to table 2 and discussed the meaning of the uncertainties.

Figures:

We took all your suggestions and improved the figures accordingly. Thank you for pointing out the parts that needed improvement. As mentioned above, we included uninterpreted photo mosaiques in the supplementary.

Implications from palaeoseismological investigations at the Markgrafneusiedl Fault (Vienna Basin, Austria) for seismic hazard assessment

Esther Hintersberger[1], Kurt Decker[1], Johanna Lomax[2,3], Christopher Lüthgens[2]

[1]Department of Geodynamics and Sedimentology, University of Vienna, 1090 Vienna, Austria
[2]Institute of Applied Geology, University of Natural Resources and Life Sciences (BOKU), 1190 Vienna, Austria
[3]Department of Geography, Justus Liebig University Gießen, 35390 Giessen, Germany

Correspondence to: Esther Hintersberger ~~(esther.hintersberger@univie.ac.at)~~(esther.hintersberger@univie.ac.at)

Abstract. ~~Including faults into seismic hazard assessment depends strongly on their level of seismic activity.~~ Intraplate regions ~~are~~ characterized by low rates of seismicity~~, so that the~~ are challenging for seismic hazard assessment, mainly for two reasons: Firstly, evaluation of ~~existing~~historic earthquake catalogues ~~does~~may not ~~necessarily~~ reveal all active faults that contribute to regional seismic hazard. Secondly, slip rates determination is limited by sparse geomorphic preservation of slowly moving faults. In the Vienna Basin (Austria), moderate historical seismicity (Imax/Mmax = 8/5.2) concentrates along the left-lateral strike-slip Vienna Basin Transfer Fault (VBTF). In contrast, several normal faults branching out ~~of~~from the VBTF show neither historical nor instrumental earthquake records, although geomorphological data indicate Quaternary displacement along those faults. Here, we present a palaeoseismological dataset of three trenches crossing one of these splay faults, the Markgrafneusiedl Fault (MF), in order to evaluate ~~the~~its seismic potential~~ of the fault.~~. Comparing the observations of the different trenches, we found evidence for 5-6 ~~major~~ surface-breaking earthquakes during the last 120 ka, with the youngest event occurring at around ~14 ka ~~before present.~~ago. The inferred surface displacements lead to magnitude estimates ranging between ~~M=~~6.2±0.~~3~~5 and ~~M=~~6.8±0.~~1~~4. Data can be interpreted by two possible ~~event lines~~slip models, with ~~event line~~slip model 1 showing more regular recurrence intervals of about 20-25 ka between the earthquakes with M≥6.5, and ~~event line~~slip model 2 indicating that such earthquakes cluster in two time intervals in the last 120 ka. ~~Event line~~Direct correlation between trenches favours slip model 2 ~~appears~~as the more plausible option. Trench observations also show that structural and sedimentological records of strong earthquakes with small surface offset have only low ~~conservation~~preservation potential. Therefore, the earthquake frequency for magnitudes between 6 and 6.5 cannot be constrained by the trenching records. Vertical slip rates of 0.~~03~~02-0.~~04~~05 mm/a derived from the trenches compare well to geomorphically derived slip rates of 0.~~015~~02-0.~~085~~09 mm/a. Magnitude estimates from fault dimensions suggest that the largest earthquakes observed in the trenches activated the entire fault surface of the MF including the basal detachment that links the normal fault with the VBTF. The most important implications of these paleoseismological results for seismic hazard assessment are that: (1) The MF ~~needs to be considered as~~is a capable seismic source ~~irrespective of~~despite the ~~fact that it did not release~~lack of historical earthquakes. (2) The maximum credible

Formatted ...
Formatted: Authors, Right: 0 cm, Space Before: 0 pt
Formatted: German (Austria)
Formatted: Authors
Formatted ...
Formatted: Font: 10 pt, Superscript, Not Raised by / Lowered by
Formatted: Affiliation, Right: 0 cm
Formatted ...
Formatted: Font: 10 pt, Superscript, Not Raised by / Lowered by
Formatted: Affiliation, Right: 0 cm, Line spacing: single
Formatted ...
Formatted ...
Formatted: Normal, Line spacing: single
Formatted: Footer

earthquakes in the Vienna Basin should be considered to be at least about M=7.0. (3) The MF is kinematically and geologically equivalent to a number of other splay faults of the VBTF. It ~~must be assumed~~is reasonable to assume that these faults are potential sources of large earthquakes as well. The frequency of strong earthquakes near Vienna is therefore expected to be significantly higher than the earthquake frequency reconstructed for the MF.

1 Introduction

During the last few years, earthquakes ~~tend~~have tended to "surprise" ~~seismologists~~the scientific community, either by unexpectedly high magnitudes (e.g., Sumatra Earthquakes 2004, Tohuko Earthquake 2011) or/and by the fact that the generating faults were either unmapped (Christchurch Earthquake 2010) or ~~assumed to be inactive~~not considered in hazard assessments (e.g., Haiti Earthquake ~~2009).~~ 2010). Thus, it seems to be clear that historical and instrumental seismicity data are not sufficient to fully characterize the seismogenic potential of a certain region (e.g., Camelbeeck et al., 2007, Liu et al., 2011). Especially in regions of low to moderate seismicity, mostly in intraplate settings, observations of historical and instrumental seismicity are not sufficient to accurately estimate the rate of earthquake activity (Liu et al., 2011). Therefore, during the last decade, geomorphological and palaeoseismological approaches have been increasingly used to map active faults and to determine the related slip rates (e.g., Clark et al., 2012, in Australia, and Vanneste et al., 2013, for the Lower Rhine graben system in Central Europe). The results of those studies have dramatically changed the picture and the ~~level~~estimation of seismogenic potential in the analysed regions, mainly in the following aspects: Firstly, palaeoseismological results show that the magnitude for the maximum credible earthquake may be significantly higher than the magnitude ~~for~~of the largest earthquake observed during historical times (e.g. Central Europe north of the Alps, Figure 1B and references mentioned there). Secondly, the ~~amount~~number of active faults that are considered to be capable of generating earthquakes ~~has been~~ increased by additional investigations (e.g., Clark et al., 2012, in Australia). The identification of such "silent" faults as potential seismic sources has become a vital aspect of geological contribution to seismic hazard assessment. Finally, ~~extension of the observed earthquake records raised the~~another important question is whether faults (especially single faults within fault systems) show regular earthquake patterns during time (~~characteristic~~quasi-periodic earthquakes ~~occuring~~occurring in more or less regular time intervals) or if earthquakes occur in ~~so-called super-cycles~~clusters, where periods of high activity ~~change~~alternate with intervals of seismic quiescence (Wallace, 1987, Friedrich et al., 2003).

Seismicity in the Vienna Basin (Austria) between the eastern margin of the European Alps and the Carpathians (see Figure 1A) seems to be nucleated at certain locations along the main active strike-slip fault, the Vienna Basin Transfer Fault (VBTF). On the other hand, several Quaternary active normal faults seem to be not seismically active. Therefore, the Vienna Basin provides a good example for firstly, addressing the question whether historical and instrumental seismicity are enough to identify active faults and secondly, analysing the behaviour of slowly moving faults in a fault system. Here, we present results of a paloseismological study~~, where~~ along a ~~dormant~~Quaternary active fault ~~has been identified~~ close to the city of Vienna

Formatted ...

Formatted: Right: 0 cm, Space Before: 0 pt

Formatted ...

Formatted: Footer

~~(Austria).~~. Even though there is no historical nor instrumental seismicity that has been recorded along this fault, three trenches across the fault show evidence for ~~five~~5-6 surface-breaking earthquakes. Correlation between the trenches and integration of geomorphological and borehole data helps to ~~identify~~distinguish whether the fault tends to more ~~characteristic~~quasi-periodic or ~~super-cycle~~clustered behaviour.

Formatted ...

Formatted: Footer

2 Geological setting

2.1 The Vienna Basin

The Vienna Basin ~~has~~ formed as a pull-apart basin between the Eastern Alps and the Western Carpathians in the Middle and Upper Miocene (e.g. Royden, 1985; Decker et al., 2005). It is located between two left-~~-~~stepping segments of the NE-SW striking sinistral strike-slip Vienna Basin Transfer Fault (VBTF, Figure ~~1~~1A). Faulting along this fault system is related to ~~the~~ NE-directed movement of the block east of the Vienna Basin, caused by lateral extrusion of the central Eastern Alps towards the Pannonian Basin (Ratschbacher et al, 1991, Linzer et al, 1997, 2002). GPS data (Grenerczy et al., 2005) and geological reconstruction of Quaternary sediment deposition within the basin (Decker et al., 2005) indicate that the VBTF moves at horizontal velocities between 1.6 and 2.4 mm/y. However, seismic slip rates calculated from cumulative scalar seismic moments for different segments along the fault are ~~quite~~ heterogeneous, varying from 0.5-1.1 mm/a at the southern and northern tips to an apparently ~~seismically totally~~ locked segment in the central part of the basin, ~~the so-called Lassee segment,~~ close to the city of Vienna (Hinsch ~~et al, 2005, Hinsch~~ and Decker, 2003, 2011). Fault mapping using 2D/3D reflection seismic, gravity, and geomorphology shows that these seismotectonically defined segments are delimited by major fault bends including a restraining bend ~~(Dobra Voda)~~at the northern end of the Vienna Basin and three releasing bends with negative flower structures overlain by Pleistocene pull~~—~~-apart basins with up to 150 m of growth strata (Beidinger and Decker, 2011). The releasing bends are connected ~~by non-transtensive~~via pure strike-slip segments.

In addition to the overall geometry of the strike-slip fault with releasing and restraining bends, the transfer of displacement to several normal faults splaying from the strike-slip system ~~in~~at the ~~central part~~edges of the ~~basin~~releasing bends appears to be an important factor controlling fault segmentation~~.~~ (Beidinger and Decker, 2011). The splay faults ~~formed~~were generated during the Middle to Upper Miocene formation of the Vienna pull-apart basin (Decker et al., 2005) and ~~seem to be~~are kinematically linked to the VBTF via a common detachment (i.e., the Alpine floor thrust, Figure 2, Hölzel et al., 2010, Hinsch and Decker, 2011, Beidinger and Decker, 2011). ~~Those~~The secondary splay normal faults ~~seem to have been~~at the central part of the Vienna Basin are considered seismically inactive during historic times~~.~~ (Figure 1A). However, geomorphologic and subsurface geophysical data reveal that ~~those~~these faults ~~indeed show~~record tens of meters of Quaternary displacement ~~of several tens of meters~~ (Chwatal et al., 2005; Decker et al., 2005, Weissl et al., 2017). -Paleoseismological trenching in the Vienna Basin was carried out so far at one of the splay normal faults, the Aderklaa-Bockfliess Fault (ABF in Figure 1A); the trench did not expose the fault, but combined electric resistivity measurements and remote sensing analysis resulted in a Quaternary slip rate of 0.05 mm/a for this fault (Weissl et al., 2017).

Moderate historical and instrumental seismicity (maximum magnitude Mmax ~ 5.3/ maximum epicentral intensity Imax = 8) is concentrated along the VBTF with the 1972 Seebenstein (M~5.3), 1906 Dobra ~~Woda~~Voda (M~5.7~~)~~), and the ~ AD 350 Carnuntum (M~6) earthquakes being the largest known events (Gutdeutsch et al., 1987; Decker et al., 2006; Lenhardt et al., 2007). The scarcity of strong earthquakes and the generally low to moderate seismicity result in Mmax estimations ~~of Mmax~~ for ~~earthquakes in~~ the Vienna Basin ~~might not exceed~~of M = 6.0 to 6.5 (Lenhardt et al., 1995; Procházková and Šimunek, 1998;

Formatted: Font: Not Bold, Font color: Auto

Formatted ...

Formatted ...

Formatted ...

Formatted: Font: 10 pt, Not Bold

Formatted ...

Formatted: Caption, Line spacing: 1,5 lines

Formatted: Footer

~~Sefara~~Šefara et al., 1998; Tóth et al., 2006). However, ~~those~~these estimations are based solely ~~based~~ on historical and instrumental seismicity.

Formatted: Font: 10 pt, Not Bold
Formatted: Font: 10 pt, Not Bold
Formatted: Font: 10 pt, Not Bold
Formatted: Font: 10 pt, Not Bold
Formatted: Font: 10 pt, Not Bold

Formatted: Footer

2.~~1~~2 The Markgrafneusiedl Fault (MF)

Our palaeoseismological study is focused on the SE-dipping Markgrafneusiedl Fault (MF) in the central part of the Vienna Basin. It is one of six ~~splay~~ normal splay faults that were ~~generated~~formed during the Middle to Upper Miocene ~~formation of the Vienna Basin~~ to accommodate transtension at a releasing bend of ~~this sinistral strike-slip fault~~the VBTF (Beidinger and Decker, 2011). The location of the fault, Miocene fault displacement and fault dimensions are evident from 2D and 3D ~~industrial~~industry seismic (Hinsch et al., 2005, Spahic et al., 2013). An exemplary seismic section is shown in Figure ~~3~~3C. Detailed observations based on 3D ~~industrial~~industry seismic data on the fault plane suggests that movement along the MF started on different fault segments that eventually merged together as one larger fault (Spahic et al., 2013). Quaternary fault reactivation is inferred from geomorphological evidence of a 12 m high linear scarp paralleling the outcrop trace of the fault, high-resolution geophysical profiling (~~georadar~~ground-penetrating radar, reflection seismic, geoelectrics; Chwatal et al., 2005) and the ca. 40 m offset of the base of the Quaternary sediments across the MF (Decker et al., 2005). The visible fault scarp ~~falls together~~coincides with the SE edge of the Pleistocene Gaenserndorf terrace~~, building~~ (Figures 3A and 4A, B). The Gaenserndorf terrace (GDT) is a ~~linear geomorphological step~~large river terrace north of ~~ca. 12 m height~~the Holocene flood plain consisting of coarse gravels in ~~the present-day topography (Figure 3).~~

sandy matrix and sandy deposits typical for braided river systems (Weissl et al., 2017 and references therein). IRSL dating suggest a minimum deposition age of 200 – 300 ka (Weissl et al., 2017). Despite ~~this~~the well documented Quaternary displacement along the MF, no historical seismicity is ~~recorded that can be~~ associated with this fault~~, except for small earthquakes with magnitudes less than 1.0 that have been recorded close to the MF in the last decade.~~. Whether this apparently slowly moving fault can produce larger earthquakes ~~or it is aseismically creeping,~~ is the key question of our study~~, during which three~~. Three trenches (from north to south WAG, SDF1, and SDF3) were excavated across the MF between the villages of Markgrafneusiedl and Gaenserndorf, about 15 km from the city limits of Vienna, the Austrian capital~~. The results show that these normal faults are indeed capable of generating earthquakes and therefore must be considered as potential seismogenic sources. In addition, the observations indicate that earthquakes within the Vienna Basin could exceed the maximum magnitudes estimated from historical and instrumental seismicity.~~ (Figures 3A and 4A).

3 Methodology

3.1 Field work

Prior to siting the trenches SDF1 and SDF3, 40 MHz ground penetration radar (GPR) profiles were carried out to locate the MF at the base of the present-day scarp (see location in Figure 4A). The chosen trench sites are located in a forested area to minimize anthropogenic influence (Figure 4C-F). The approximately N(W)-S(E) trending trenches were excavated for about

Formatted: Not Expanded by / Condensed by , Not Raised by / Lowered by

Formatted: Not Raised by / Lowered by

Formatted: Not Expanded by / Condensed by , Not Raised by / Lowered by

Formatted: Not Raised by / Lowered by

Formatted: Footer

40-50 m with the NE wall benched (Figure 4D, F). Both walls were covered by a grid of 0.5 m x 0.5 m with rows named from A (top) to J and L (bottom), respectively, and columns counted from 1 at the SE end upwards to the NW end. Photomosaiques of all walls were obtained by taking pictures of two grid rectangles (1 m x 0.5 m) and subsequent manually ortho-rectifying and stitching in ArcGIS. Trench logging was conducted at a scale of 1:10 for the entire (S)W walls of the trenches and the section around the fault zone on the (N)E walls.

3.2 Luminescence dating

Luminescence dating is commonly used to date the time that feldspar grains in sandy or silty sediments were not exposed to sunlight, and therefore to constrain deposition ages of those sandy or silty sediment bodies. Regarding the physical background and the basics of luminescence dating methods we refer to previously published reviews of Preusser et al. (2008), Wintle (2008), and Rhodes (2011). In analogy to the procedure described by Weissl et al. (2017), samples were collected in the field by driving an opaque steel cylinder into the freshly cleaned sediment surface and transferring the material into light tight plastic bags. All subsequent sample preparation steps were conducted under subdued red light conditions in the Vienna laboratory for luminescence dating. Samples were first dried and dry sieved. The grain size fraction of 100 - 200 mm was used for further preparation steps. Potassium-rich feldspar was used as luminescence dosimeters for age determination. All fractions were measured with multi-grain aliquots of 1 mm diameter mask size. All measurements for determination of the equivalent dose were conducted in the Vienna laboratory for luminescence dating on RISØ TL-OSL DA 20 automated luminescence reader systems (Bøtter-Jensen et al., 2000, 2003). For De determination of the feldspar fraction, a conventional SAR IRSL protocol was applied (Wallinga et al., 2000; Blair et al., 2005), using a preheat of 250°C for 20 s and a stimulation at 50°C for 300 s. Stimulation was carried out with IR-LEDs, and signals were detected after passing through a blue interference filter (410 ± 20 nm). Over-dispersion (Galbraith et al. 1999) was below 11% in all samples confirming a generally well-bleached nature of the sediments. Radionuclide concentrations for dose-rate estimation were determined on ~900 g of bulk sediment using high resolution, low-level gamma-spectrometry. Samples were first dried, homogenised and stored in sealed Marinelli beakers (500 ml, about 1 kg dry weight) for at least a month to establish secondary secular radon equilibrium. Measurements were conducted using a Canberra HPGe detector (40% n-type). Relevant luminescence data is listed in Table 1.

It needs to be stressed that the feldspar based ages were not corrected for fading. Fading describes an anomalous signal loss very commonly observed for potassium-rich feldspar (Wintle, 1973). If not corrected for, fading leads to the underestimation of the burial age. However, samples from the same study area investigated by Weissl et al. (2017) showed little or no fading, as demonstrated by a comparison between quartz and feldspar luminescence ages. Nevertheless, all ages presented here need to be treated with caution for potential age underestimation.

Formatted: Footer

3.3 Modelling occurrence times and recurrence intervals

For the calculation of earthquake occurrence times and recurrence intervals, we used the Bayesian statistical computer program OxCal v4.3.2 (Bronk Ramsey, 1995, 2001). Each trench is modelled separately as a chronological sequence with the respective IRSL dating results in stratigraphic order constraining the earthquake occurrence times. IRSL dating results are initially represented as uniform distributions covering the respective errors. In a next step, the chronological sequences of all trenches are combined by the "Phase"command, so that the constraints from all trenches for each single earthquake occurrence time are considered at the same time. Intervals between earthquakes are calculated using the command "Difference". Detailed code information is given in the supplementary.

Formatted: Footer

4 Trenching results

~~In total, we~~We excavated two trenches along the geomorphic fault scarp between the villages of Markgrafneusiedl and Gaenserndorf (~~Figure~~Figures 3A~~). For the exact position of the trenches, 40 MHz ground penetration radar (GPR) profiles were carried out showing the location of the MF at the base of the present-day scarp.~~ and 4). In addition, the third trench consists of a construction ~~pit~~trench of a gas pipeline ~~exposed~~exposing the northern tip of MF~~,~~ and providing additional, but limited, information. In general, all outcrops show similar characteristics: at all trenching locations, the MF is exposed as a narrow (1 - 2 m) fault zone consisting of one or two fault branches striking parallel to the regional strike of the fault scarp of the MF (dip direction/dip: ~120/75). The footwall cut by the MF comprises deposits typical ~~for~~of the Pleistocene Gaenserndorf terrace ~~(Weissl et al., 2017 and references therein).~~. The hanging wall of the trenches expose sequences of almost horizontally layered, fine-~~graded~~grained sediments of probably fluvial and lacustrine origin intercalated with colluvium deposited discontinuously during the last 160 ka. High-resolution photomosaiques of trenches SDF1 and SDF3 are provided in the supplementary.

Formatted: Footer

34.1 Trenching at SDF1

The 40-m-long, 3-m-wide and up to 4 m deep trench SDF1 was located close to the farm house "Siehdichfür", about 20 km from the city limits of Vienna. (Figures 3A and 4A). It was excavated in a small dry valley at the central part of the NE-SW trending geomorphological fault scarp with the exact location of the MF at its base. Trench mapping in the scale of 1:10 covers both, the entire SW wall of the trench and the section around the fault zone at the NE wall.. The trench SDF1 exposed about 30 m of Gaenserndorf terrace deposits in the footwall and ca. 10 m of mostly fine-graded sandy to silty sediments the hanging wall, divided by the 1.5 m wide fault zone of the SE-dipping MF. The fault zone includes two parallel steeply dipping faults F1 and F2, with F2 reaching almost the present-day surface (see Figure 45).

At the NW part in the footwall, alluvial deposits of the Gaenserndorf terrace are exposed, consisting of poorly sorted coarse gravels and boulders. in a grain-supported sandy matrix (U2). Pebbles show consistent NW-dipping imbrication throughout the entire footwall section. The inferred dominantly SE-directed paleocurrents are comparable to the flow direction of the Recent Danube. In addition, two approximately 8 m wide sandy ancient river channel fills are observed close to the topA lense of the succession. Anothermedium light grey sand lense, onlywith mm-size white mica minerals (U1 in Figure 5), partly exposed at the base of the outcroptrench bottom, is cut by the fault zoneF2. The uppermost 0.5 m of the terrace depositsdeposit directly below the recent soil horizon dodoes not show any horizontal consistency and are mostis probably reworked and repositioned.

In the hanging wall SE of the fault zone, three types of sediments are exposed:

(A) Sequences of horizontal layers of light-grey and light-brown silt and fine sand with varying thicknesses up to 20 cm. (Units U3, U4, U7). Sediments show lamination on cm-scale and intercalations of cm-thick horizons of coarse sand. The layers also include singular well-rounded pebbles and granules aligned in horizontal layers. Some sand/silt layers show fining-upward trends. Carbonate cementation is observed along the top of the uppermost silt layer and along recent root paths. The sediments are intercalated with and onlap on the wedge-shaped colluvial deposits described below. We relate the deposits to high-stage floods in the floodplain of the Pleistocene Danube.

(B) Colluvial wedge deposits (W2-W5 in Figure 5) and associated tension crack fills. (T2-T4 in Figure 5). These colluvial sediments are attachedadjacent to both faults and decrease in thickness towards the SE (i.e., away from the fault scarp;, Figure 46B). The steep contact with the SE-dipping faults and the thinning of the deposits towards SE results in a wedge-shape of the sediment layers. The tails of wedges 2, 3W2, W3 and 5W5 can be followed throughout the exposed part of the hanging wall. All wedges are associated with tension cracks adjacent to the fault,faults (T2-T4), which are filled with the same material as the overlying wedge. Wedge 5, but showing no preferred orientation. The lowest wedge W5 consists of matrix-supported reddish brown medium gravel with a matrix composed mainly by sand and silt together with a low content of clay. Wedge 4 isThe overlying wedge comprises two parts, W4 and W4a, delimited by a steep irregular boundary adjacent high-stage flood sediments. While wedge 4 comprisesW4 consists of brown to reddish brown fine to medium sand with some fine granules and pebbles in a matrix-supported fabric, the latterW4a include rounded pebble-size clasts of the reddish wedge material interpreted

Formatted: Not Expanded by / Condensed by , Not Raised by / Lowered by

Formatted: Footer

as mud balls. (Figure 6C and E). We interpret this peculiar contact to result from the partial erosion of the wedge and the wedge tail during high-stage floods and the re-deposition of the colluvial material by fluvial processes or small slumps. Wedge 3W3 consists of well-sorted reddish brown middlemedium-grained sand with a few pebbles (fine gravel) showing lamination dipping away from Fault 1. These three wedges contrast by their fault F1 (Figure 6C). The red and reddish-brown colour of W3-W5 contrasts from the light grey-beige intercalated high-stage flood deposits. The sedimentary wedge material was identified as redeposited soil, which bybecause its colour, resembles ferretto soils (5YR 4/4, Y5YR 5/4 and 5YR 58 of the standard soil colour chart; L. Smolíková, pers. comm.), which derived from the.). The source for the redeposited soil would be the previous soil cover of the terrace gravels in the footwall of the MF. While the lower three colluvial wedges (3-5)W3, W4, and W5 are bounded by F1, wedge 2W2 is attachedadjacent to F2 and overlies the trace of F1as well as the W3 deposits of wedge 3. The wedge. W2 consists of large well-rounded pebbles and cobbles oriented sub-horizontally in a grain-supported fabric, similar to the terrace deposits found in the foot wall. On top of W2 and U2, a paleo-soil has been developed after deposition of W2, visible by black and brownish colouring of the upper 25 cm (Figures 5 and 6A, B). The underlying tension crack T2 is composed by the same material, but with slightly larger cobbles with no horizontal layering.

(C) Fine-grained alluvium (units U5, U6, U8) and loess. The uppermost part of the sedimentary succession of (U9) found in both the hanging wall and the footwall consists of several thin layers of sand and fine gravel overlain by up to 1 m of unstructured silt and fine sand. (U10). The latter is transitional to the overlying dark brown to black soil horizon. (U11). The succession is interpreted as alluvium of the dry valley and loess-like sediments or redeposited loess. Fault 2 offsets the alluvial sand layers (U5, U6, U8) for about 15 to 20 cm, but terminates within the overlying loess-like sediments of U10 several cm above the base of the layer. (Figure 6A).

Structural data obtained from the two faults exposed in the outcrop show that both faults strike parallel to the regional str ikestrike of the fault scarp of the MF. The faults are marked by bands of rotated pebbles with preferred orientations parallel to the fault pla nesplanes. Pebbles in the 75 cm thick fault block between the two faultsF1 and F2 show orientations, which geometrically resemble S--C-type fabrics. Deformation bands are found in the sand wedges 3sandy deposits of W3 and 4W4, and the related tension cracks. T3 and T4 (Figure 6c). Detailed mapping reveals that these microfaults do not penetrate into the colluvial wedge 5W5 most probably due to the higher clay content of these sediments. The deformation bands show orientations consistent with the main faults of the outcrop. At the lower parts, the deformation bands are dippingdip parallel to F1 (dip direction/dip 130/80). The upper parts of the deformation bands are rotated away from the fault resembling horsetail splays. The orientations of the sub-vertical deformation bands vary between 303/78 and 330/78. In addition to some major deformation bands, which are traced for about 1 m across the profile, there are shallow dipping deformation bands with comparably large normal offsets up to several mm (145/20). Finally, small-scale normal faults with displacement in the order of several centimeterscentimetres are observed within the uppermost layers that have been also affected by the youngest displacement along F2units U6-U8 (Figure 5E5 and 6D).

Formatted: Footer

34.1.1 Evidences for seismic events observed within trench SDF1

Slip events identified in SDF1 will be labelled as A1-A5 from the youngest to the oldest. Offset of alluvial sand layersunits U5, U6, and U8 at the tip of F2 provides direct evidence for the youngest surface-breaking slip event A1. (Figure 6A). The small-scale faults observed in the same units U6, U7, and U8 (Figure 6D) are at the same stratigraphic level are further indications for an earthquake at this fault. A1 is offsets and postdates colluvial wedge 2.and indicate faulting within the hanging wall during A1. Neither F2 nor the small faults cut units 9 and 10. In addition, W2 has been also offset by A1 along F2, clearly seen by the coloured paleo-soil (Figure 6A). The observed colluvial wedges W2-W5, their geometrical relation to the adjacent faults, and the sediment tension cracks (T2-T4) filled extension fissureswith same material prove four distinct events (A2 to A5) of rapid co-seismic displacement at the MF. In addition, the existence of deformation bands within the sandy colluvial wedges 3deposits of W3, T3, W4, and 4T4 indicates further deformation of both wedges during younger slip event, either A1 or, more probably A2.

Due to the subhorizontal layering within the hanging wall, the occurrence of the events at the MF. Among the A2, A3, and A5 can be bracketed by sediments lying below and above the respective wedge tails. The deposits of W2 lie directly on top of W3 (Figures 5 and 6B). The associated earthquakes excavated by the trench, only slipA2 and A3 must have occurred after the deposition of U4 and before U5 and U6 were deposited. A5 must have occurred between the deposition of units U3 and U4. The colluvial wedge associated with A1 is directly A4 has been partly eroded (W4 and W4a), which must have happened during the deposition of U4. Therefore, A4 must have happened after the occurrence of A5 and before the deposition of U4.

Direct measurement of offset is only possible for A1, which is constrained by the offset of layers correlated across Fault 2. fault F2, i.e., units U5 and U6 and the top of W2. The 1.5 m of apparent offset of U5 and U6 awayEvidence for the earthquakes A2 to A5 comes from the colluvial wedges 2fault between the top of the footwall and SE end of the hanging wall due to 5 and the refilled tension cracks 2'the sedimentation on pre-existing topography, and not related to 5' below the wedgesafterslip. Following the generally accepted rule of thumbs that colluvial wedge height is approximately half of the surface displacement of an earthquake (McCalpin, 2008), the measured maximum thickness of each colluvial wedge W2-W5 can be used to estimate the minimum displacement for the associated event. (Table 2).

3.2 Trenching at SDF3

Trenching in the Vienna Basin continued with the opening of a 4.1.2 Age control at SDF1

The fine-graded sandy and silty subhorizontal deposits of the hanging wall of trench SDF1 provide good dating material for IRSL dating. We sampled the sandy sediments in stratigraphic positions below and above the tails of the colluvial wedges A5, and A2/A3. In addition, we took samples from unit 7 which is affected by faulting related to A1, and from unit U10 sealing fault F2. In general, luminescence dating results fit well to the stratigraphic hanging wall sedimentary sequences observed in the trench, showing continuous decrease in age from the bottom towards the top (Figure 5 and Table 1). In addition, the age derived for the Gaenserndorf terrace in the footwall fit well with other ages from this terrace (Weissl et al., 2017).

Formatted: Font: +Body (Times New Roman)

Formatted: Footer

Event A1 is well constraint between the IRSL dating results derived for unit 10 (13.8 ± 1.4 ka) and unit 7 (16.3 ± 1.8 ka) by samples from an offset sand layer and overlying undeformed sediments. Events A2 and A3 are bracketed by the ages of unit 7 (16.1 ± 1.7 ka) and the uppermost sediments of unit U4 below W2/W3, which were dated to 48.9 ± 4.8 ka. The occurrence times of A4 and A5 are constraint by the ages of the lowest sediments of U4 (56.6 ± 5.7 ka) and the age of deposits of U3 (104 ± 12 ka) below the W5, the stratigraphically lowest sediments in the hanging wall.

4.2 Trenching at SDF3

We opened the second trench SDF3 ~~across the same fault.~~about 1.5 km SW of trench SDF1 (Figure 3A and 4A). This 33 m long, 3 m wide and up to 5 m deep trench ~~is~~was located ~~about 1.5 km SW of the first trench SDF1. Trench mapping in the scale of 1:10 covers both, the entire W wall of the trench and the section around the fault zone exposed in the terraced E wall (Figure 6~~along a clearing in the forest (Figure 4). The about 0.5 m wide fault zone of the SE-dipping MF divides the N-S trending trench into two parts. The footwall W of the fault mainly consists of gravels of the Gaenserndorf terrace whereas the hanging wall in the E shows a succession of fluvial sediments, colluvial deposits originating from the uplifted footwall and reworked ~~loess-like~~silty sediments~~.~~ (Figure 7).

The footwall ~~mainly~~ consists of poorly sorted, well rounded sandy gravels within a grain-supported fabric. ~~Components mostly~~The clasts include metamorphic rocks, gneisses, quartzite along with minor sandstone and limestone. The few magmatic components found within the gravels are completely weathered. The lower 1-1.5 m of the terrace ~~excavated~~exposed in the trench contains coarse cobbles with diameters up to 25 cm~~.~~ (U1). The upper part shows typical characteristics of ~~braded~~braided river deposits, including crossbedding of ~~better~~good-sorted gravel layers intercalated with sand layers of up to 0.5 m of thickness and several meters of lateral extent~~.~~ (U2). Furthermore, this part consists of gravel and small cobbles with diameters up to 10 cm. All layers show a slight inclination towards the SE. Throughout the terraces deposits, vadose gravitational carbonate cementation~~, so-called~~ ("dripstone cementation~~,~~") along the lower side of larger gravels is observed.

The hanging wall consists of horizontally layered ~~sediments of different origin~~fluvial, probably alluvial, and erosional deposits. In the following, we describe the most important units of the hanging wall, starting with the lowermost unit. Unit ~~1~~4 consists of intercalated beige to grey, medium to fine sand, and gravel layers ~~consisting of~~comprising well-rounded, poorly sorted clasts. The thickness of the layers varies between ~3 cm and 20 cm, whereas the sand layers are generally thicker than the intercalated gravel layers. This sequence is the result of alternate high-stage Danube floods (sand layers) and erosional events transporting gravels from the footwall into the hanging wall. ~~Those erosional impulses may be triggered by heavy rainfall events. The contact to the overlying unit 2 is clearly identified. Unit 2 consists~~Colluvial wedge W5 is bound by F3 towards the N, decreases in thickness towards the SE and disappears approximately 3.5 m away from the fault zone. W5 consists of matrix-supported conglomerate with a sandy matrix and poorly sorted, well-rounded clasts. On top of W5, separated by a sand layer of few centimetres, deposits of colluvial wedge W4 spreads through the whole hanging wall. The W4 deposits consist of matrix-supported conglomerate with clay-rich, Fe-rich red fine sandy matrix and poorly sorted, well-rounded clasts with

Formatted: Footer

diameters up to 15 cm. Grain sizes decrease with increasing distance from the fault, as well as the layer thickness from 70 cm directly at the fault to less than 50 cm further away~~.~~ (Figure 8A). The contact to the overlying unit ~~3~~U5 is ~~diff use. Unit 3~~diffuse. U5 consists of red clay-rich Fe-rich fine sand with intercalated layers and up to 5 cm thick lenses of brownish slightly coarser sand without clay or Fe components. The layering shows a slight inclination of a few ~~degree~~degrees towards the NW, i.e., towards the fault. The material is typical for distal flood basin deposits of fluvial environments. A few well rounded clasts with diameters of 2 - 20 cm ~~have been~~were observed~~. Their distribution suggests~~ that ~~they may be~~we interpret as dropstones~~.~~ (Figure 8B). Furthermore, an animal burrow of small animals, refilled with beige coarse sand is observed at the bottom of this layer. The contact between this unit and the overlying unit ~~4~~U6 is characterized by a ~~generally~~ horizontal sharp contact, which has been affected by liquification, either caused by ~~the occurrence of~~ an earthquake or by ~~the~~ deposition of the overlying coarse gravels over the still water-bearing sediments of ~~unit 4. Furthermore, a burrow of small animals, refilled with beige coarse sand is observed at the bottom of this layer. Unit 4~~U5 (Figure 8B, C). Close to the fault, there are several wedge-shaped deposits between U5 and U6. W3 is exposed for about 3 m in the hanging wall close to the fault. It consists of approximately 25 cm thick gravels and small cobbles with diameters up to 10 cm. On top of W3, a package of layered sediments dips towards S (W2). Its thickness close to F1 is about 0.8 m and decreases within 1 m away from the fault. The layers consists of well-sorted pebbles, partly without matrix (red layer). W2 is then covered with U6. U6 consists of grain-supported conglomerate with well-rounded, poorly sorted cobbles with grain sizes up to 10 cm. Those gravels originate from the footwall and form a colluvial wedge, which decreases in thickness with increasing distance to the fault. Unit ~~5~~U7 consists olive-coloured medium sand with rare mica components. This 10 cm thick unit decreases in thickness towards the fault. This fact, together with the colour of the sand, suggests that it is a flood deposits of the Danube. Unit ~~6~~U8 covers both, the hanging and the foot wall and consists of a matrix-supported conglomerate with silt matrix and around 25% of components that consist of poorly sorted, well-rounded pebbles with grain sizes up to 3 cm. The silt matrix consists of reworked loess that has probably eroded from the footwall, including smaller clasts from the Gaenserndorf terrace. In the top of this unit, secondary carbonate cemented a horizontal layer of up to 30 cm thickness. The layer is observed throughout the entire hanging wall. Carbonate cementation occurs due to meteoric waters ~~dissipating~~dissolving carbonate from the upper layers and precipitating it at lower pH values in greater depth. Conjugated planar carbonate fissures of up to 60 cm length branch off from the cemented layer. They strike approximately parallel to the orientation of the MF. Unit ~~7~~U9 is the AC soil horizon, consisting of a matrix-supported conglomerate of fine sand and 30-40% of components containing partly angular and rounded pebbles with grain sizes up to 2 cm. The contact to both, the underlying and overlying units~~,~~ is rather diffuse. Finally, unit ~~8~~U10 is the A soil horizon that increases in thickness with increasing distance ~~to~~from the MF. Its thickness coincides with a layer of silt or loess that has been reworked as soil.

Structural data obtained from the outcrop show that both faults strike parallel to the regional strike of the fault scarp of the MF (dip direction/dip: 116/74). The MF is marked by the contact between the footwall gravels and the more sandy deposits of the hanging wall. In addition, at the lower 1.5 m, clasts within a zone of about 50 cm to the fault are rotated parallel to the fault (~~dip direction/dip:~~ 116/69). The upper part of the MF is ~~only~~ marked by a small band of rotated ~~clasts.~~clast (F1). However, in

Formatted: Footer

this upper part of the fault, layers that can be correlated on both sides of the fault, are displaced by about 15 cm~~ and, therefore, indicate the youngest~~, indicating movement along ~~the fault~~F1. In addition to the main ~~faults~~fault strands F1-F3, several conjugated sets of normal faults are observed within lower units of the hanging wall. These faults are consistently oriented parallel to the MF. The NW-dipping antithetic faults (~~dip direction / dip: ~~303/79) are generally longer than the SE-dipping faults (~~dip direction / dip: ~~137/72). Displacement observed along the faults is in the range of about 10 cm in ~~the lowest unit 1~~U4, and up to 1 cm in ~~the reddish clay-rich unit 3. None of the small faults seem to penetrate into the gravels overlying the reddish clay-rich sand layer (unit 3).~~U5. Within this layer, the small faults are recognised as a few mm thin deformation bands, most probably filled with carbonate cement, and show almost no displacement. None of the small faults seem to penetrate into the gravels of U6. The sand layers of ~~the lowermost unit 1~~U4, consisting of intercalated layers of sand and matrix~~-~~supported gravels, comprises small deformation bands with lengths up to 20 cm. They are arranged parallel to the small faults and accordingly dip towards the SE or the NW.

~~3~~4.2.1 Evidences for seismic events observed within trench SDF3

Single slip events identified in SDF3 are labelled as B1-B5. The MF within the trench SDF3 is a~~ very~~ narrow fault zone of 0.5 m width at its lowest point excavated within the trench, and reduces to a fault represented only by a few rotated clasts in the uppermost part~~. However, this ~~ (F1). This reduction of thickness ~~is not a continuous, but ~~occurs in distinct steps~~. Those steps~~ which can be related to different earthquakes~~:~~. The oldest earthquake ~~that can be~~B5 is identified within the trench ~~is B5 that~~ created a colluvial wedge W5 along the fault trace F3. This fault trace is then covered by another colluvial ~~wege~~wedge W4, which was most probably created by movement along F2 during ~~B4.~~earthquake B4. W5 and W4 are bracketed between the hanging wall units U4 and U5. Evidence for ~~the ~~event B3 is a tension crack T3 between F2 and F2', that is also identified by the thin sand layer that is smeared into the crack, parallel to F2'. ~~B2 is identified by a ~ 0.8 m thick colluvial wedge.~~W3 is most probably deposited before the occurrence of B3, and the material was smeared into the fault zone along F2' during B2. As the deposits of W3 partly cover the deposits of U5, the occurrence of B3 must be later than U5. The primary evidence for B2 is the ~ 0.8 m thick colluvial wedge W2 (Figure 7, 8A). However, the fault strand bounding this colluvial wedge is not obvious. This situation may be explained by the following scenario: In the case that coseismic surface rupture offset unconsolidated water-saturated sandy gravel, it seems plausible that no long-standing free surface and colluvial wedge adjacent to the fault plane could form. Instead, the offset soft sediment may have collapsed during or shortly after the earthquake forming a wedge-shaped deposit, which overlies the uppermost part of the ruptured fault. The same geometry may result from geli-solifluction under periglacial conditions when material glides down to the hangingwall destroying a free surface previously formed ~~free surface~~by B2. The latter scenario is supported by the observation of a smooth change between the horizontal layers of the terrace and the inclined layers in the colluvial wedge. The described situation allows for two different interpretations of the surface displacement of B2. Interpreting the wedge-shaped deposit as a classical colluvial wedge adjacent to a fault plane which is not readily seen due to unfavourable outcrop conditions, a minimum displacement can be estimated by multiplying

Formatted: Footer

the maximum wedge height by two (McCalpin, 2008), which ~~would result in a~~suggests displacement of 2 x 0.8 m = 1.6 m for B2. ~~In~~For the case ~~that the~~of wedge ~~formed~~formation by free surface collapse of water-saturated sediment or gelifluction, the coseismic surface displacement would be approximately the same as the colluvial wedge height, i.e. 0.80 m. We consider the latter scenario as the more fitting one and therefore use 0.80 m as the preferred value for the surface displacement for B2. Since B2 is directly on top of unit W3, and is covered by the gravels of U6, its occurrence can be bracketed between the deposition of units U5 and U6, similar to B3. Insights for the youngest event B1 in the trench are ~~more~~the most obvious. Displacement of ~~the upper layers for~~ ~ 10 cm along F1 affected all layers excluding only the soil horizons (~~units 7~~U9 and ~~8~~U10), suggesting that even with such a small displacement of ~~only~~ 10 cm, ~~the~~ event B1 ruptured the surface~~.~~ (Figure 8A).

~~3.3 Trenching~~4.2.2 Age control at SDF3

The fine-graded sandy deposits of U3 (AIP93, 158 ± 21 ka), U4 (AIP95, 123 ± 16 ka), U5 (between 111 ± 12 ka, AIP95 and 70.8 ± 8.0 ka, AIP97), U7 (32.9 ± 4.1 ka, AIP98) and U10 (4.8 ± 0.5 ka, AIP102) in the hanging wall provide material suitable for IRSL sampling. The dating results (details see Table 1) follow the chronological order of the sedimentary deposits well. In addition, two samples from sand lenses within unit U2 (AIP103 and AIP114) determine the minimum age of the footwall to 205 ± 37 - 259 ± 35 ka. Those obtained ages agree well with other IRSL ages for the Gaenserndorf terrace (Weissl et al., 2017). The IRSL data of the hanging wall constrain roughly the occurrence times of the 5 observed paleo-earthquakes along the main fault. B1 has affected U6 and the base of U8, and therefore also U7, constraining its occurrence after 32.9 ± 4.1 ka. As units U9 and U10 seal F1, B1 must have occurred before 4.8 ± 0.5 ka. As mentioned above, B2 and B3 are bracketed between units U7 and the top of U5, limiting its occurrence time between 32.9 ± 4.1 ka and 70.8 ± 8.0 ka. B4 and B5 are also jointly constraint between the deposition of unit U4 (111 ± 12 ka) and the base of U5 (123 ± 16 ka)

4.3 Outcrop WAG

Additional evidence for active faulting at the MF ~~are~~is available from the construction pit of a gas pipeline, which crosses the northern part of the fault scarp close to the city of Gaenserndorf, 6 km north of trench SDF1~~.~~ (Figure 3A). The outcrop revealed a 1-m-wide localized fault zone (~~Figure 8).~~ Figures 9, 10A)The fault cuts light-grey gravel and sand of the Gaenserndorf Terrace and overlying ~~loess-like sediments (silt,~~approximately 1 m thick fine-graded silty to ~~medium grained sand)~~sandy deposits constituting its footwall. The exposed hanging wall succession includes poorly sorted sandy ~~gravel~~gravels, which is then overlaid by a banded sequence of silty sediments. This cover layer can be found all along the pipeline construction pit and has been described in detail by Weissl et al. (2017). Two IRSL samples from fine-graded silty to sandy cover were dated to ages of 15.1 ± 1.5 ka and 16.1 ± 1.7 ka, respectively (samples AIP25, 26, Table 1), giving the only time constrain at the WAG site. Both the hanging wall and footwall are overlain by c. 30-50 cm thick brown soil, which has been removed prior to ~~the~~ excavation. The exposed fault zone consists of several ~~deformation bands~~faults within the terrace gravel marked by aligned and fractured pebbles, faults offsetting sand layers, and faults offsetting the contact between gravel units and the overlying

Formatted: Not Expanded by / Condensed by , Not Raised by / Lowered by

Formatted: Not Expanded by / Condensed by , Not Raised by / Lowered by

Formatted: Keep with next

Formatted: Footer

cover silts (Figure 9 and 10B, C). Several sheared pebbles indicate dip--slip movement along the deformation bands.faults (Figure 10D, E). The displacements of these faults are between 10 and 20 cm. On the southernSW wall, a fault cuts up through the entire silty section to the base of the overlying soil, offsetting a thin white layer within the upper part of the cover silty sediments by about 20 cm.20 cm (Figure 10A). This offset indicates evidence for the youngest earthquake at the WAG site, C1. This earthquake must have happened after the deposition of the silty cover sediments, i.e. after 15.1 ± 1.5 ka. In Figure 10A, the poorly sorted sandy gravels in the hanging wall form a wedge-shaped deposit close to the fault (marked with CW). This can be interpreted as a colluvial wedge associated to an earthquake C2 that occurred before the deposition of the silty cover sediments. Therefore, C2 must be older than 16.1 ± 1.7 ka. Since the base of the colluvial wedge is not identifiable, a displacement of C2 cannot be assessed.

4 Luminescence dating

Luminescence dating is commonly used to date the time that feldspar and/or quartz grains in sandy or silty sediments were not exposed to sunlight, and therefore to constrain deposition ages of those sandy or silty sediment bodies. Regarding the physical background and the basics of luminescence dating methods we refer to previously published review papers of Preusser et al. (2008), Wintle (2008), and Rhodes (2011).

4.1 Sampling and experimental setup

In analogy to the procedure described by Weissl et al. (2017), samples were collected in the field by driving an opaque steel cylinder into the freshly cleaned sediment surface and transferring the material into light tight plastic bags. All subsequent sample preparation steps were conducted under subdued red light conditions in the Vienna laboratory for luminescence dating. Samples were first dried and dry sieved. The grain size fraction of 100 - 200 mm was used for further preparation steps. The material was subjected to 15% HCl to remove carbonates, treated with Na2C2O4, (0.01 N) to disperse clay particles, and with 10% H2O2 to dissolve organic components. Quartz and feldspar separates were obtained by density separation using LST Fastfloat.

In this study, we used potassium-rich feldspar as luminescence dosimeters for age determination. All fractions were measured with small aliquots of 1 mm diameter mask size using a grain size fraction of 100 - 200 mm. All measurements for determination of the equivalent dose were conducted in the Vienna laboratory for luminescence dating on RISØ TL-OSL DA 20 automated luminescence reader systems (Bøtter-Jensen et al., 2000, 2003). For De determination of the feldspar fraction, a conventional SAR IRSL protocol was applied (Wallinga et al., 2000; Blair et al., 2005), using a preheat of 250°C for 20 s and a stimulation at 50°C for 300 s. Stimulation was carried out with IR-LEDs, and signals were detected after passing through a blue interference filter (410 ± 20 nm). Doses were determined on small multi-grain aliquots (mask-size 1mm). Over-dispersion (Galbraith et al. 1999) was below 11% in all samples confirming a generally well-bleached nature of the sediments. It needs to be stressed that the feldspar based ages were not corrected for fading. Fading describes an anomalous signal loss very

Formatted: Footer

commonly observed for potassium-rich feldspar (Wintle, 1973). If not corrected for, fading leads to the underestimation of the burial age. However, samples from the same study area investigated by Weissl et al. (2017) showed little or no fading, as demonstrated by a comparison between quartz and feldspar luminescence ages. Nevertheless, all ages presented here need to be treated with caution for potential age underestimation. Radionuclide concentrations for dose-rate estimation were determined on ~900 g of bulk sediment using high resolution, low-level gamma-spectrometry. Samples were first dried, homogenised and stored in sealed Marinelli beakers (500 ml, about 1 kg dry weight) for at least a month to establish secondary secular radon equilibrium. Measurements were conducted using a Canberra HPGe detector (40% n-type). Relevant luminescence data is listed in Table 2.

4.2 Sedimentary and tectonic context

In general, luminescence dating results fit well to the stratigraphic hanging wall sedimentary sequences observed in both trenches, showing continuous decrease in age from the bottom towards the top. In addition, ages derived for the Gaenserndorf terrace in the footwall fit well with other ages from this terrace (Weissl et al., 2017).

Regarding to trench SDF1, Event A1 is well constraint between 13.8 ± 1.4 ka and 16.3 ± 1.8 ka by samples from an offset sand layer and overlying undeformed sediments. Events A2 and A3 are bracketed by the ages inferred for A1 and the undeformed sediments below the colluvial wedge related to A3 and therefore occurred between 16.1 ± 1.7 ka and 48.9 ± 4.8 ka. The ages of A4 and A5 are similarly constrained in the trench SDF1 by sediments below and above the colluvial wegdes. Both events occurred between 56.6 ± 5.7 ka and 104 ± 12 ka.

In trench SDF3, samples (AIP93-AIP102) defining the chronology of the stratified hanging wall between 158 ± 21 ka and 4.8 ± 0.5 ka were dated in addition to two more samples (AIP103 and AIP114) determine the minimum age of the footwall to 205 ± 37 - 259 ± 35 ka. Those obtained ages agree well with other IRSL ages for the Gaenserndorf terrace (Weissl et al., 2017). In addition, IRSL data of the hanging wall constrain roughly the occurrence times of the 5 observed paleo-earthquakes along the main fault. While B1 is constrained to have occurred between 4.8 ± 0.5 ka and 32.9 ± 4.1 ka, B2 and B3 can only limited to occur together within the time interval between 32.9 ± 4.1 ka and 70.8 ± 8.0 ka. Also for B4 and B5, a common time interval between 111 ± 12 ka and 123 ± 16 ka can be determined. At the trench site WAG, both the uppermost and the lowermost sediments of the fine-graded silty to sandy cover were dated by IRSL revealing ages of 15.06 ± 1.52 ka and 16.1 ± 1.7 ka, respectively (samples AIP25, 26, Weissl et al., 2017).

Formatted: Footer

5 Correlation of events between sites

Palaeoseismological investigations along the MF include three locations, the trenches SDF1 and SDF3 as well as the pipeline outcrop WAG. For all three locations, detailed mapping and dating have been carried out and described above. Evidence for ~~5~~five possible earthquakes have been observed in the trenches SDF1 (named A1-A5) and SDF3 (B1-B5), while in the pipeline ~~outcrop~~trench WAG, observations indicate two paleo-earthquakes (C1 and C2). ~~-~~Table 2 summarizes the observations, time constraints and occurrence times for each earthquake and each trench separately. The central panel of Figure ~~10~~11 shows the constraints of earthquake occurrence times for each ~~observation point.~~trench separately. Based on this information, together with comparison of trench observations and displacement estimates for all three outcrops, we correlate ~~the~~trench observations and occurrence timing results to generate a synthesis of ~~the~~ earthquake occurrence along the MF. In the following, we discuss each earthquake and the possible correlations between the trenches as well as the resultant ~~age~~occurrence time, displacement and magnitude estimate, starting with the youngest. The summary of this discussion is shown in Table 3.

5.1 Event ~~1~~E1 (A1 = B1 = C1)

In all three ~~outcrops~~excavations, the youngest event is evident from a measurable offset of layers across the MF. At trench site SDF1, the youngest event A1 shows displacements of 15-25 cm ~~and occurred in the~~(Figure 6A). Its occurrence time ~~range~~is bracketed between 13.8 ± 1.4 ka and 16.3 ± 1.8 ka. At trench site SDF3, markers have been displaced by the youngest event B1 by 10-15 cm~~. The~~ (Figure 8A). ISRL ~~data~~dating results limits the occurrence time of B1 to the time range between 4.8 ± 0.5 ka and 32.9 ± 4.1 ka. In the pipeline ~~outcrop~~trench WAG, the loess cover is dated between 15.1 ± 1.5 ka and 16.1 ± 1.7 ka. It is displaced by 17-20 cm~~.~~, visible by a white marker within the loess (Figure F10A). Therefore, C1 must have happened after 15.1 ± 1.5 ka.

~~The~~Combination of constraints for E1 from all three sites yields to an occurrence time ~~for E1 is thus constraint to the time interval between 13~~of 14.2 ± 0.8 ~~± 1.4~~ ka ~~and 15.1 ± 1.5 ka (Table 2).~~. Using the ~~empiric~~empirical relationship between surface displacement and magnitude (Wells and Coppersmith, 1994) for the maximum displacement of 25 cm, ~~E1 had~~ the magnitude estimate for E1 is $M(d_{max})$ = 6.2 ± 0.~~2~~5. The average displacement of 17 cm would lead to a similar magnitude ~~M~~estimate of $M(d_{ave})$ = 6.3 ± 0.~~3~~6.

5.2 Event ~~2~~E2 (A2 = B2 = C2)

Event E2 is also observed ~~in~~at all three ~~outcrops~~sites as a triangular-shaped colluvial wedge mainly consisting of reworked gravels ~~that~~ derived from the terrace in the footwall~~.~~ (Figures 6B, 8A, 9). In addition, the ~~top of each of those~~ colluvial ~~wedge~~wedges deposits ~~is~~related to A2 and B2 are displaced by the younger event E1, confirming the correlation of the colluvial wedges to the penultimate seismic event E2. At trench site SDF1, the displacement related to A2 (1.5-1.9 m) is estimated from the height of the associated colluvial wedge (0.75 - 0.95 m). IRSL samples from sediments above and below the colluvial wedge constrain the occurrence time for A2 ~~to the time interval~~ between 16.1 ± 1.7 ka and 48.9 ± 4.8 ka. At trench site SDF3,

Formatted: Font: Not Bold, Font color: Auto

Formatted: Not Expanded by / Condensed by , Not Raised by / Lowered by

Formatted: Not Expanded by / Condensed by , Not Raised by / Lowered by

Formatted: Font: +Body (Times New Roman), English (United States)

Formatted: Font: +Body (Times New Roman), English (United States)

Formatted: Not Expanded by / Condensed by , Not Raised by / Lowered by

Formatted: Not Expanded by / Condensed by , Not Raised by / Lowered by

Formatted: Font: +Body (Times New Roman)

Formatted: Footer

the interpretation of deposits related to B2 are more ambiguous (see sec. 3.2), and therefore, the estimated displacement is either 0.8 m (collapsed free face scenario) or 1.6 m (colluvial wedge scenario). B2 is constrained between 32.9 ± 4.1 ka and 70.8 ± 8.0 ka~~.~~ by the IRSL ages of sediments above and below the colluvial wedge material. In the pipeline construction ~~pit~~trench WAG, the displacement of E2 ~~can only be~~is not constrained~~ to exceed 1 m by the colluvial wedge as~~, because the base of the wedge ~~is~~was not ~~exposed. Time constraints are limited to the ante quem~~excavated. The maximum age of 16.1 ± 1.7 ka ~~by~~for the ~~age of the overlying~~ loess covering the colluvial wedge~~.~~ gives a minimum age for the occurrence of C1.

Combining the ~~individual~~ time constraints ~~in each~~from all trench ~~site~~sites allow to determine the occurrence time of E2 ~~between 32.9~~to 37.1 ± 4.~~1 ka and~~ 9 ~~48.9 ± 4.8~~ ka. Magnitude calculation using the maximum of the observed surface displacements results in a magnitude of M(d_{max}) = 6.8 ± 0.~~1)~~4 (Wells and Coppersmith, 1994). With the maximum value for the observed surface displacement coming from trench SDF1, the magnitude estimate does not depend on the interpretation for the B2 deposits in trench SDF3.

5.3 Event ~~3~~E3 (A3, probably correlated with B3)

For this event, a correlation based on field observations between the trenches SDF1 and SDF3 is not as clear as in the cases of E1 and E2, especially since the evidence for B3 does not allow to determine a displacement for this ~~possible~~ event. However, the maximum height of a well-developed sandy colluvial wedge in SDF1 gives a good estimate of an earthquake with M(d_{max}) = 6.6 ± 0.~~1.~~4 (Figure 6C). Because of the similar stratigraphic constraints, the combined possible occurrence time of E3 ~~is constrained by the same limits as E2, so~~at 43.4 ± 4.9 ka overlaps with that ~~E3 occurred also between 32.9 ± 4.1 ka~~ one of E2 (Figure 11, lower and ~~48.9 ± 4.8 ka.~~upper panels).

5.4 Event ~~4~~E4a (A4, if correlated with B3)

~~Another~~Due to the loose time constraint of B3, another possible correlation scenario between the trench sites SDF1 and SFD3 is the correlation of events A4 and B3 (~~event line~~slip model 1 in Figure ~~10), mainly due the loose time constraint of B3.~~11, upper panel). If A4 and B3 are correlated to the same seismic event ~~E4~~E4a, the overlap of possible occurrence times of A4 and B3 narrows the resultant occurrence time for ~~E4~~E4a to ~~the interval between 56.6~~64.9 ± 5.~~7 ka and 70.8 ± 8.0~~ 6 ka. Observations of the maximum wedge height at trench site SDF1 indicate the magnitude of A4 (and therefore for ~~E4~~E4a) to M = 6.8 ± 0.~~2~~5.

5.5 Event ~~5~~E4b (A4, if correlated with B4)

In an alternative scenario, A4 could also correlate to B4 (~~event line~~slip model 2 in Figure ~~10~~11, lower panel). In this case, the combined occurrence time for the resultant seismic event ~~E5~~E4b must be older than the 111 ± 12 ka old sediments below the wedge associated with B4 in trench SDF3 (Figure 7) and younger than the lowest sediments in trench SDF1 dated to 104 ± 12 ka~~.~~ (Figure 5). Thus, the time ~~constraint~~constraints for E4b would ~~be thigh, dating E5 to the overlap~~lead to a narrow time

Formatted: Font: +Body (Times New Roman), English (United States)

Formatted: Font: +Body (Times New Roman), English (United States)

Formatted: Not Expanded by / Condensed by , Not Raised by / Lowered by

Formatted: Not Expanded by / Condensed by , Not Raised by / Lowered by

Formatted: Not Expanded by / Condensed by , Not Raised by / Lowered by

Formatted: Not Expanded by / Condensed by , Not Raised by / Lowered by

Formatted: Left

Formatted: Font: +Body (Times New Roman), German (Austria)

Formatted: Font: +Body (Times New Roman), German (Austria)

Formatted: Not Expanded by / Condensed by , Not Raised by / Lowered by

Formatted: Not Expanded by / Condensed by , Not Raised by / Lowered by

Formatted: Left

Formatted: Footer

window for its occurrence of ~~the uncertainties of the IRSL age dating between 100~~106 ± 3 ka ~~and 116 ka with a mean at 107.9 ± 8.0 ka.~~. Similar to ~~E4~~E4a, the magnitude for ~~E5~~E4b can be estimated from the observations of the maximum wedge height of A4 at trench site SDF1, indicating a magnitude for ~~E5~~E4b of M = 6.8 ± 0.~~2~~5.

5.6 Event ~~6~~E5a (possible correlation between A5 and B4) and Event ~~7~~5b (possible correlation between A5 and B5)

The ~~later~~further back in time, the more uncertain the correlation between both trench sites becomes. So, whether A5 and B5 are correlated to one event ~~E6~~E5a, or A5 and B4 are correlated to one event ~~E7~~E5b is not clearly determined neither by observations nor dating. Both alternatives are possible and only depend on whether A4 is correlated to B3 or to B4. In ~~event line~~slip model 1~~,~~ (Figure 11, upper panel), where A4 ~~s~~is correlated with B3, it appears reasonable to assume subsequently that A5 ~~=~~equals to B4. In contrast, if A4 ~~=~~is correlated with B4 (~~event line~~slip model 2, Figure 11, lower panel), the remaining correlation for the next older event would be that A5 ~~=~~corresponds to B5. Due to the loose time constraints in the lower part of all trenches, the ~~occurrence times~~ available chrono-stratigraphic constraints for ~~E6~~E5a and ~~E7~~E5b are identical to those used for ~~E5, leading to a time window~~E4b (Figure 11, central panel). However, additional constraints of ~~approximately 100–116 ka where either E6 or E7 occurred.~~chronological order demand that E5a and E5b must have happened earlier than E4a and E4b, respectively. This yields to slightly different occurrence times of 107 ± 4 ka and 109 ± 3 ka for E5a and E5b, respectively. Since both magnitude estimates for ~~E6~~E5a and ~~E7~~E5b are based on the maximum colluvial wedge height of A5 from trench SDF1, the magnitude of ~~E6~~E5a and ~~E7~~E5b is M = 6.5 ± 0.~~1)~~4.

5.7 Event ~~8~~E6a (B5, if not correlated with any event in SDF1)

~~In~~For the case that B5 is not correlated with any events recorded in trench SDF1 (~~event line~~slip model 1), the timing of ~~E8~~E6a would be bracketed by the ~~age~~IRSL dating ~~s~~results of 111 ± 12 ka and 123 ± 16 ka. ~~E8 would therefore slightly older than E6 and E7. This would also imply that E8~~In addition, with A5 (=E5a) being the oldest earthquake evidence in SDF1, E6a might be older than the oldest deposits in SDF1 and therefore not visible there. Both time constraints yield to an occurrence time of 120 ± 7 ka for E6a. Unfortunately, the magnitude of this possible seismic event cannot be constrained by trench observations.

6 Seismotectonic implications

6.1 Completeness and preservation potential of earthquake records along the MF

The comparison between the evidences for youngest surface breaking earthquake E1, which did not lead to the formation of colluvial wedges, and the older events, which are characterized by larger offsets and colluvial wedges throughout, raises the question on the completeness of the paleoseismological earthquake record. It seems that the colluvial wedges associated with larger earthquakes that rupture the same surface-breaking fault conceal or even erase evidence for samller offsets by earthquakes such as E1. The displacement of the markers by E1 is only preserved because the event happened after the last

Formatted: Font: +Body (Times New Roman), German (Austria)

Formatted: Font: +Body (Times New Roman), English (United States)

Formatted: Not Expanded by / Condensed by , Not Raised by / Lowered by

Formatted: Not Expanded by / Condensed by , Not Raised by / Lowered by

Formatted: Not Expanded by / Condensed by , Not Raised by / Lowered by

Formatted: Not Expanded by / Condensed by , Not Raised by / Lowered by

Formatted: Not Expanded by / Condensed by , Not Raised by / Lowered by

Formatted: Footer

earthquake (E2) that caused a colluvial wedge to form. Any future event with a surface displacement that is large enough to lead to the erosion of the offset markers in the footwall will destroy the evidence for E1.We conclude that this restriction also applies to earthquakes with small surface offset that occurred prior to E2. Therefore, earthquake records for magnitudes less than about 6.5 are most probably incomplete, and thus excluded from the recurrence calculation.6.1

6.2 Recurrence intervals for earthquakes with magnitudes larger than 6.5 along the MF

The possible correlations of paleoearthquakes between the trenches allow for two different interpretations to reconstructassess the recurrence intervals of earthquakes with magnitudes larger than M = 6.5. The event E1 will be excluded during the following considerations, since the related magnitude estimate is lower than those obtained for E2-E7. It seems that the colluvial wedges associated with the larger earthquakes conceal or even erase evidences for offsets formed by smaller earthquake. The displacement of markers related to E1 is only conserved because the event happened after the last earthquake that caused a colluvial wedge to form (E2). Any future event with a surface displacement that is large enough to lead to the erosion of the offset markers in the footwall will destroy the evidence for E1. This restriction also applies to earthquakes with small surface offset that occurred prior to E2. E5a/b. Therefore, earthquake records for magnitudes less than about 6.5 are most probably incomplete, and thus excluded from the recurrence calculation.

As mentioned in sect. 5, the crucial part for the reconstruction of recurrence intervals therefore is whether A4 is correlated either to B3 or to B4 and, subsequentlyconsequently, whether A5 is correlated to B4 or to B5, resulting in the following event linesslip models:

(Slip model 1): E2-E3(not correlated to B3)-E4-E6-E8E4a-E5a-E6a (5 earthquakes);

(Slip model 2): E2-E3(correlated to B3)-E5-E7E4b-E5b (4 earthquakes).

The determination of inter-event intervals is based on the limits for the occurrence time intervals for each earthquake as given in Table 2. Figure 10 shows clearly that both event lines represent different types of distributing earthquakes. Event line 1 represents an approximately periodic reoccurrence of earthquakes with magnitudes larger than M = 6.5. The maximum time interval between E2 and E3 is 15.8 ka. As the occurrence time of E3 limits the occurrence time interval of E2, the minimum time interval cannot be calculated. Considering event line 1 (E2-E3-E4-E6-E8) and the range of uncertainties related to dating, the inter-event time between E3 and E4 lies between 6.3 ka and 41.5 ka, while the inter-event time between E4 and E6 is between 20.2 ka and 65.1 ka. Finally, the maximal inter-event time between E6 and E8 is constrained to 40 ka. Similar to the inter-event time for E2/E3, a minimum inter-event time for E6/ E8 cannot be calculated. Taking all information together, the average of the minimum values and the average of the maximum recurrence intervals for event line 1 would be then ~ 13 ka and ~ 40 ka, respectively.

On the other side, earthquakes in event line 2 (E2-E3-E5-E7) seem to cluster in time. Therefore, instead of calculating inter-event times for all earthquakes, we calculate the minimum inter-cluster time that is identical with the inter-event time for E3/E5, and the maximum intra-cluster times for E2/E3 and E5/E7, meaning the largest possible time between both

Formatted: Not Expanded by / Condensed by , Not Raised by / Lowered by

Formatted: Footer

earthquakes within the same cluster. A maximal inter-cluster time cannot be given, due to the poor time constraint within the both clusters. However, the maximal intra-cluster times for E2/E3 and E5/E7 are 15.8 ka and 17.0 ka, respectively. In addition, the minimum inter-cluster time interval between E2/E3 and E5/E7 is at least 54.4 ka. The time since the occurrence of E2 until today may be also considered as a minimum inter-cluster time, being at least 32.9 ± 4.1 ka and maximal 40.9 ± 3.6 ka. Another estimation of the minimum elapseRecurrence intervals are calculated using OxCal v.4.3.2 (Bronk Ramsey, 1995, 2001) and the results are shown in Figure 12. Despite the large uncertainties, the plots show that the slip models may represent different types of earthquake distributions.

Slip model 1 (E2-E3-E4a-E5a-E6a) shows a quasi-periodic recurrence of earthquakes with magnitudes larger than M = 6.5 with an average recurrence interval of 21 ± 15 ka (mean ± 1σ). The most likely elapsed time between E4a and E5a (42 ± 7 ka) is significantly higher than the average, and that one between E2 and E3 (6.2 ± 4.6 ka) is significantly lower than the average (see Figure 12, upper panel). The probability distribution for the interval between E3 and E2 peaks at 0, because the occurrence times of E3 and E2 are limited by the same stratigraphic constraints. Because of the large variation of recurrence intervals for slip model 1, an estimate about the expected next M≥6.5 earthquake along the MF is difficult to make. However, considering the elapse time of 37 ± 5 ka since the last M≥6.5 earthquake, E2, is above the average, the likelihood of an earthquake of this magnitude along the MF should be considered high.

For slip model 2 (E2-E3-E4b-E5b), the average recurrence interval of 24 ± 34 ka is predictably similar to that of slip model 1, but with a larger standard deviation. However, the distribution of earthquake recurrence intervals in slip model 2 differs significantly from slip model 1 by showing a bimodality (Figure 12, lower panel). As mentioned above, the probability distribution for the interval E2/E3 peaks at 0, and so does the interval for E4b/E5b. The most likely interval between E3/E4b (63 ± 6 ka) is 10-20 times larger than those for E4b/E5b (3.2 ± 2.6 ka) and E2/E3 (6.2 ± 4.7 ka). Inferring a clustered behaviour for earthquakes along the MF for slip model 2, the average cluster length would be 4.7 ± 3.8 ka. The elapsed time interval between clusters E2/E3 and E4b/E5b corresponds to the interval E3/E4b. In addition, the time since the occurrence of E2 until today can be also considered as a minimum time between clusters (37 ± 5 ka). Furthermore, another estimation of the minimum time between clusters can be estimated from the oldest layers in trench SDF3 (unit 8) dated to 158 ± 21 ka (sect. 3.2). Since there is no older record than B5, it is reasonable to assume that there was no earthquake during the time between B5 and the oldest unit 8 exposed in SDF3. Therefore, the minimum time elapsed between B5 (=E7) and any older cluster must be at least 42 ± 21 ka.E5b) and any older cluster must be at least 49 ± 13 ka. The average recurrence interval between clusters would be therefore at least 49 ± 13 ka. Adopting slip model 2 and assuming that M≥6.5 earthquakes cluster along the MF may lead to the presumption that the MF is in between clusters at the moment. Because the time since the last cluster (37 ± 5 ka) is below the average recurrence interval for clusters, the likelihood of a M≥6.5 earthquake along the MF might be considered low at the moment, with the next cluster most likely to occur in approximately 10 ka.

Formatted: Footer

6.~~1~~3 Comparison of long-term Quaternary slip rates with paleoseismological slip rates

Paleoseismological vertical slip rates are calculated based on trench observations. In trench SDF1, the total sum of displacement is 4.85 ± 0.50 m, using the minimum displacement obtained mostly from colluvial wedge heights (Table 2). As the oldest sediments in trench SDF1 are 104 ± 12 ka old, the resultant vertical slip rate is 0.05 ± 0.01 mm/a. For trench SDF3, this straight forward calculation is not possible, because there is no displacement estimate for the older three earthquakes. However, since the terrace top is not seen in the hanging wall, the difference in elevation of 3.5 m between the top of the terrace in the footwall and the bottom of the trench, can be used as a minimum displacement. Together with the IRSL dating results for the oldest sediments in the hanging wall 158 ± 21ka, the resultant minimum vertical slip rate for SDF3 is 0.02 mm/a. The slip rate for the last two earthquakes B1 and B2, where displacement estimates are available, the vertical slip rate would be between 0.02-0.05 mm/a for the time since E2 (37 ± 5 ka) using either 0.9 m (E1 + free face collapse) or 10.8 m (E1 + colluvial wedge).

Long-term Quaternary slip rates ~~**along**~~of the MF can be ~~**inferred**~~estimated from ~~**using**~~ the ~~**morphological scarp height**~~offset of ~~**about 17 m and the age of**~~two marker horizons, the top of the Gaenserndorf terrace ~~**(~ 200 ka, Weissl et al., 2017). Using the present-day scarp height as minimum displacement**~~ and the base of the Quaternary deposits. The top of the Gaenserndorf terrace forms the current land surface in the footwall of the MF. As the top of the Gaenserndorf terrace is not exposed in the hanging wall sections of the trenches, and thus is buried below the present-day surface at the hanging wall, the height of the morphological scarp of about 17 m (Figure 3B) represents minimum displacement accumulated since the abandonment of the fluvial terrace 200 ka ago~~, a~~ (Weissl et al., 2017),. The resulting minimum Quaternary slip rate ~~of~~is 0.~~085~~09 mm/a ~~**may be assumed. In addition, the**~~.

The base of the Quaternary gravels in the hanging wall of the MF, which is equivalent to the top of Neogene sediments, is offset by approximately 40 m ~~**(Figure 3). Assuming that this should**~~ with respect to the base of the Gaenserndorf terrace in the footwall of the MF (Figure 3B). In the absence of age information for the gravels in the hanging wall of the MF and the bottom of the Gaenserndorf terrace, the oldest available age for the Gaenserndorf terrace, 322 ± 41 ka (Weissl et al., 2017), is used for estimating a maximum long-term slip rate for the MF of 0.12 mm/a. A minimum slip rate of 0.02 mm/a is calculated from the 40 m displacement of the Quaternary gravels which must have ~~**happened**~~accumulated after the Neogene-Quaternary boundary (2.6 Ma~~**), the slip rate along the MF should be larger than 0.015 mm/a. It must be noted that this is a minimum estimate since age data from the thick Quaternary sediments in the hangingwall of the MF are not available. Figure 11**~~). Figure 13 shows the range of possible slip rates for both ~~**event lines**~~slip models falling in between the bracket of the geomorphic slip rates, ~~**showing a**~~which are in reasonable agreement.

Formatted: Not Expanded by / Condensed by , Not Raised by / Lowered by

Formatted: Font: 10 pt, Not Bold

Formatted: Font: 10 pt, Not Bold

Formatted: Font: 10 pt, Not Bold

Formatted: Font: 10 pt, Not Bold

Formatted: Font: 10 pt, Not Bold

Formatted: Font: 10 pt, Not Bold

Formatted: Font: 10 pt, Not Bold

Formatted: Font: 10 pt, Not Bold

Formatted: Font: 10 pt, Not Bold

Formatted: Font: 10 pt, Not Bold

Formatted: Font: 10 pt, Not Bold

Formatted: Font: 10 pt, Not Bold

Formatted: Font: 10 pt, Not Bold

Formatted: Font: 10 pt, Not Bold

Formatted: Caption, Line spacing: 1,5 lines

Formatted: Font: 10 pt, Not Bold

Formatted: Font: 10 pt, Not Bold

Formatted: Font: 10 pt, Not Bold

Formatted: Font: 10 pt, Not Bold

Formatted: Font: 10 pt, Not Bold

Formatted: Footer

~~**6.3 Recurrence intervals for earthquakes with magnitudes larger than 6.5 along the MF**~~

6.4 Comparison of magnitude estimates with fault rupture area and length

For faults with known fault geometry, ~~empiric~~empirical relations allow to evaluate the maximum magnitude that a fault can produce from rupture length and area. The surface expression of the MF is only recognizable for about 10 km along the eastern margin of the Pleistocene Gaenserdorf terrace (Figure 3A). Further to the south, the River Danube has erased any geomorphic expression in its Holocene flood plain. However, the geometry and the length of the MF are well known ~~thanks to~~from the distribution of Quaternary sediments in the ~~hangingwall~~hanging wall of the fault and 2D/3D reflection seismic ~~within the central Vienna Basin~~ (Hölzel et al., 2010, Hinsch and Decker, 2011, Salcher et al., 2012, Spahic et al., 2013). ~~Based on these~~These data~~,~~ constrain the length of the MF ~~as an isolated fault is around~~to 25 km (Salcher et al., 2012). In addition, Hinsch and Decker (2011) ~~constructed~~proposed a generalized detachment for the Vienna Basin~~.~~ (see Figure 2). Beneath the MF, the detachment is assumed to be at the depth of about 10 km (Wessely et al., 2006). Taking into account the general dip of 55° for the MF observed in seismic lines, the rupture area of the MF above the detachment would amount to 315 km², leading to a maximal credible magnitude of 6.5 ± 0.3~~)~~.

However, in case that the MF is indeed linked to the VBTF via the common detachment as proposed by Beidinger and Decker (2011), the area of the detachment between the MF and VBTF might be also activated during large events (Figure ~~12~~14). The total fault surface activated during such events is derived as the sum of the fault surface of the MF and the portion of the basal detachment between the MF and the VBTF, which has a size of about 130 km². The fault length of the MF in this tectonic scenario is 36 km and the total fault area amounts to about 580 km². These fault parameters correspond to a maximal credible magnitude of 6.7 ± 0.3~~)~~ for earthquakes along the MF using the relationships ~~by~~of Wells and Coppersmith (1994~~). This~~), which is in good agreement ~~to~~with the paleoseismological magnitude estimations derived from ~~the~~our trenches.

6.5 Mmax for the Vienna Basin

Previous estimates of the maximum earthquake (Mmax) for the Vienna Basin are based on the evaluation of historical and instrumental seismicity only and present values for Mmax between M = 6.0 to 6.5 (Lenhardt et al., 1995; Procházková and Šimunek, 1998; Sefara et al., 1998; Tóth et al., 2006). In contrast to these assessments, the results of our study suggest that earthquakes with magnitudes up to about M=7.0 are likely to occur on longer time scales. Based on the data from the MF presented here, a value of Mmax=7.0 should be considered in seismic hazard studies as a minimum. Considering that the MF and the other splay normal faults are connected to the VBTF via the common detachment (Figures 2 and 14), a possible combined rupture along the MF and the VBTF would increase the Mmax for the Vienna Basin. Hinsch and Decker (2011) present different rupture scenarios along the VBTF with Mmax in the order of 5.9-6.8 for single-segment ruptures of different strike-slip segments of the VBTF. The assumption of scenarios such as earthquakes rupturing several strike-slip segments or events rupturing parts of the VBTF combined with secondary rupture along one of the splay normal faults would definitively increase the Mmax. However, there is not enough data so far to prove or disprove any of those scenarios.

Formatted: Font: 10 pt, Not Bold

Formatted: Caption, Line spacing: 1,5 lines

Formatted: Font: 10 pt, Not Bold

Formatted: Font: 10 pt, Not Bold

Formatted: Font: 10 pt, Not Bold

Formatted: Font: 10 pt, Not Bold

Formatted: Font: 10 pt, Not Bold

Formatted: Font: 10 pt, Not Bold

Formatted: Font: 10 pt, Not Bold

Formatted: Footer

7 Conclusions and implications for seismic hazard assessment

In this study, we provide evidencereport constrains for the seismogenic characterpaleoseismological history of a splay normal fault of the VBTF that previously has not been considered as a source for seismic hazards.hazard calculations. We show evidence that the fault causedproduced at least 5-6 strong earthquakes with magnitudes larger than 6.2 in the last 120 ka. The magnitude of the earthquake with the largest surface displacement is evaluated with 6.8 ± 0.1).4. This value compares well with the maximum magnitude of 6.7 ± 0.3) estimated from the potential rupture area of the MF. The fault area is about 580 km² when including the detachment that links the normal fault with the VBTF. The vertical fault slip velocityrate of 0.0302 to 0.0405 mm/a derived from trench observations liesagrees well withinwith the geomorphologically determined vertical slip rates for the MF, which range from 0.08509 to 0.01502 mm/a.

Trench observations and uncertainties of OSL/IRSL age dating do not allow for an unequivocal conclusion of earthquake recurrence rates. BothTwo earthquake scenarios (event lines, referred to as slip models 1 and 2) presented here, are possible considering the available time constraints. Event line and the possible correlations between identified paleoearthquakes in the three trenches (Figure 11). Among these, slip model 1, however, appears less likely as it seems improbable that an earthquake with a magnitude around 6.6 has not been recorded in trench SDF3, while producingit produced a surface displacement of 80-90 cm in trench SDF1 at a distance of less than 2 km. For us, the more plausible correlation between the trenches is therefore event lineslip model 2, suggesting that earthquakes with magnitudes larger than 6.5 cluster in time. This may have consequences for the application of the reconstructed recurrence intervals in seismic hazard assessments, e.g., by using cluster recurrence intervals rather than average single event recurrence intervals.

Trench evidence for the youngest event E1 (magnitude 6.2 ± 0.25) further showssuggests that strong earthquakes with magnitudes less than about 6.5 can also occur outside of the suggestedproposed clusters. Unfortunately, the recurrence intervals of such events cannot be constrained by trenching results. The sedimentary and structural records of events with surface displacements, which are too small to produce colluvial wedges, may be masked or even erased by subsequent larger earthquakes that lead to the erosion and redeposition of material into colluvial wedges. Therefore, earthquake records for magnitudes less than about 6.5 are most probably incomplete at the MF.

The issues discussed above lead us to conclude the following main implications for seismic hazard assessment in the Vienna Basin:

Basin:

1. 1. The paleoseismological results from demonstrate that the MF prove that it is seismically active and needs toshould be considered as a seismogenic source in seismic hazard assessment. Earthquakes with magnitudes larger than about 6.5 occur at average recurrence times of about 25 ka (event lineslip model 1), or, more likely, in clusters (event linemay be clustered (slip model 2; Figures 1011 and 1112). The frequency of surface-breaking earthquakes with magnitudes less than about 6.5 along the MF cannot be constrained by the trenching results due to the low

Formatted: List Paragraph, Numbered + Level: 1 + Numbering Style: 1, 2, 3, … + Start at: 1 + Alignment: Left + Aligned at: 0,63 cm + Indent at: 1,27 cm

Formatted: Footer

preservation potential of such earthquake records~~.~~ within the excavated trenches. The data presented in our study was used in the SHARE project to incorporate the MF in its active fault database (Basili et al., 2013).

2. ~~2.~~ Data from the MF provides evidence that a value of at least M=7.0 should be adopted for the maximum credible ~~earthquakes~~earthquake (Mmax) in the Vienna Basin~~ should not be considered to be about M=7.0~~. This value is significantly higher than previous estimates of Mmax = 6.0 to 6.5 (Lenhardt et al., 1995; Procházková and Šimunek, 1998; Sefara et al., 1998; Tóth et al., 2006). ~~The data presented in our study was used in the SHARE project to incorporate the MF in its active fault database and hazard calculation (Basili et al., 2013).~~We stress that the value obtained from the MF only characterizes one out of a number of secondary normal faults to the VBTF. The VBTF may produce even larger earthquakes.

3. ~~3.~~ The MF is kinematically and geologically ~~equivalent~~analogous to a number of other splay normal faults of the VBTF close to the Austrian capital, Vienna (~~Figure 9~~Figures 1 and 14; Beidinger and Decker, 2011). It ~~must be assumed~~is prudent to assume that these faults are potential sources of large earthquakes as well. However, except for the Aderklaa-Bockfliess faults (Weissl et al., 2017),~~ no~~ paleoseismic characterisation of these faults ~~exists so far.~~has yet to be conducted. The frequency of strong earthquakes near Vienna is therefore expected to be ~~significantly~~ higher than the earthquake frequency reconstructed for the MF.

4. ~~4.~~ The magnitude of the largest earthquake recorded at the MF (6.8 ± 0.~~1~~4) is regarded to support the assumption of a listric fault and an active basal detachment that links the normal fault with the VBTF strike-slip system. ~~This fault geometry has severe~~The consequences of this geometry may be large for ~~the~~ ground motion ~~pattern related to~~patterns resulting from earthquakes that activate large parts of the listric fault with ground motion expected to be more severe in the hanging wall direction, than in the footwall direction (Passone and Mai, 2016). Although such directivity effects may reduce the hazard arising from the MF for Vienna, the opposite is true for other listric faults stretching into the city limits of Vienna (Figure ~~12).~~14).

Acknowledgements

We wish to thank Dana Tschegg and all other colleagues who helped us to gain a deeper understanding of the paleoseismology of the MF by their discussion in the trenches, among them G. Bokelmann, M. Fiebig, C. Grösel, A. Landgraf, W. Lenhardt, P. Spacek, K. Reicherter, P. Štěpančíková, M. Strecker, and K. Vanneste. Thanks to E. Brückel, W. Chwatal, and K. Roch for their geophysical support and M. Meghraoui, who shared his morphological expertise in the site selection process. We further appreciate the hands-on support of many students of the Department of Geodynamics during the trenching action. Thanks also to P. Havlíček and L. Smolíková for analysing paleosoil from trench SDF1. Finally, we want to thank the three reviewers whose thoughtful and detailed reviews helped shape the manuscript into its present form. This research was funded by the Austrian Bundesministerium für Land- und Forstwirtschaft, Umwelt und Wasserwirtschaft, BMLFUW-UW-.1.1.4/00009-V/6/2009.

Formatted: German (Austria)

Formatted: Footer

References

ACORN, 2004. Seismic active discontinuities in the region “Eastern Alps-Western Carpathians-Bohemian Massif” based on geophysical data and digital seismic records of the seismic network “ACORN”. W. A. Lenhardt (ed.), Federal Ministry for Education, Science and Culture, Vienna, 2004.

Basili R., Kastelic V., Demircioglu M. B., Garcia Moreno D., Nemser E. S., Petricca P., Sboras S. P., Besana-Ostman G. M., Cabral J., Camelbeeck T., Caputo R., Danciu L., Domac H., Fonseca J., García-Mayordomo J., Giardini D., Glavatovic B., Gulen L., Ince Y., Pavlides S., Sesetyan K., Tarabusi G., Tiberti M. M., Utkucu M., Valensise G., Vanneste K., Vilanova S., Wössner J., The European Database of Seismogenic Faults (EDSF) compiled in the framework of the Project SHARE. http://diss.rm.ingv.it/share-edsf/, doi:10.6092/INGV.IT-SHARE-EDSF, 2013.

Beidinger, A. and Decker, K., 3D geometry and kinematics of the Lassee flower structure: Implications for segmentation and seismotectonics of the Vienna Basin strike–slip fault, Austria, Tectonophysics, 499, 22-40, doi:10.1016/j.tecto.2010.11.006, 2011.

Blair M.W., Yukihara, E.G., and McKeever, S.W.S., Experiences with single aliquot OSL procedures using coarse-grain feldspars, Radiat. Meas., 39, 361-374, 2005.

Bøtter-Jensen, L., Bulur, E., Duller, G.A.T., and Murray, A.S., Advances in luminescence instrument systems, Radiat. Meas., 32, 523–528, 2000.

Bronk Ramsey, C., Radiocarbon Calibration and Analysis of Stratigraphy: The OxCal Program, Radiocarbon 37, 425-430, 1995.

Bronk Ramsey, C., Development of the Radiocarbon Program OxCal, Radiocarbon 40, 461-474, 2001.

~~Cabral J., Camelbeeck T., Caputo R., Danciu L., Domac H., Fonseca J., García-Mayordomo J., Giardini D., Glavatovic B., Gulen L., Ince Y., Pavlides S., Sesetyan K., Tarabusi G., Tiberti M. M., Utkucu M., Valensise G., Vanneste K., Vilanova S., Wössner J., The European Database of Seismogenic Faults (EDSF) compiled in the framework of the Project SHARE. http://diss.rm.ingv.it/share-edsf/, doi:10.6092/INGV.IT-SHARE-EDSF, 2013.~~

Camelbeeck, T., Alexandre, P., Vanneste, K. and Meghraoui, M., Long-term seismicity in regions of present day low seismic activity: the example of Western Europe. Soil Dyn. Earthq. Eng., 20, 405-414, 2000.

Camelbeeck, T. and Meghraoui, M., Geological and geophysical evidence for large palaeo-earthquakes with surface faulting in the Roer Graben (northwest Europe). Geophys. J. Int., 132, 347-362, 1998.

Camelbeeck, T., Vanneste, K., Alexandre, P., Verbeeck, K., Petermans, T., Rosset, P., Everaerts, Warnant, R., and van Camp, M., Relevance of active faulting and seismicity studies to assessments of long-term earthquake activity and maximum magnitude in intraplate northwest Europe, between the Lower Rhine Embayment and the North Sea. Geol. Soc. Am. Spec. Pap. 425, 193-224, 2007.

Chwatal, W, Decker, K., and Roch, K.-H., Mapping of active capable faults by high-resolution geophysical methods: examples from the central Vienna Basin. Austrian J. Earth Sci., 97, 52-59, 2005.

Formatted: Footer

Clark, C., McPherson, M, van Dissen, R., Long-term behaviour of Australian stable continental region (SCR) faults. Tectonophysics, 566-567, 1-30, 2012.

Decker, K., Gangl, G., and Kandler, M., The earthquake of Carnuntum in the 4th century AD - archaeologic results, seismologic scenario and seismo-tectonic implications for the Vienna Basin Fault, Austria. J. Seismol., 10, 479-495, 2006.

Decker, K., Gruppe, S. and Hintersberger, E., Characterizing active faults in the urban area of Vienna, Miscellanea INGV, 27, 212-215, 2015

Decker, K., Peresson, H., and Hinsch, R, Active tectonics and Quaternary basin formation along the Vienna Basin Transform fault. Quaternary Sci. Rev., 24, 305-320, 2005.

Friedrich, A. M., Wernicke, B. P., Niemi, N. A., Bennett, R. A., and J. L. Davis, Comparison of geodetic and geologic data from the Wasatch region, Utah, and implications for the spectral character of Earth deformation at periods of 10 to 10 million years, J. Geophys. Res., 108, 2199, B4, doi:10.1029/2001JB000682, 2003.

Galbraith, R.F., Roberts, R.G., Laslett, G.M., Yoshida, H., and Olley, J.M., Optical dating of single and multiple grains of quartz from Jinmium rock shelter, northern Australia: Part I, experimental design and statistical models. Archaeometry, 41, 339-364, 1999.

Gutdeutsch, R., Hammerl, C., Mayer, I., and Vocelka K., Erdbeben als historisches Ereignis – Die Rekonstruktion des niederösterreichischen Erdbebens von 1590. Springer Verlag Wien, Heidelberg, New York, 1987.

Grenerczy, G., Sella, G., Stein, S., and Kenyeres, A., Tectonic implications of the GPS velocity field in the northern Adriatic region. Geophys. Res. Lett., 32, L16311, doi: 10.1029/2005GL022947, 2005.

Grünthal, G.., Wahlström, R. and Stromeyer, D., The unified catalogue of earthquakes in central, northern, and northwestern Europe (CENEC) - updated and expanded to the last millennium. J. Seismol., 13, 517-541, 2009.

Hinsch, R., Decker, K., and Wagreich, M., 3-D mapping of segmented active faults in the southern Vienna Basin. Quaternary Sci. Rev., 24, 321-336, 2005.

Hinsch, R. and Decker, K., Seismic slip rates, potential subsurface rupture areas and seismic potential of the Vienna Basin Transfer Fault, Int. J. Earth Sci. (Geol. Rundsch.), 100, 1925 -1935, doi:10.1007/s00531-010-0613-3, 2011.

Hölzel, M., Decker, K., Zámolyi, A., Strauss, P., and Wagreich, M., Lower Miocene structural evolution of the central Vienna Basin (Austria). Mar. Petrol. Geol., 27, 666-681, doi:10.1016/j.marpetgeo.2009.10.0052010.

Lenhardt, W. A., Regional earthquake hazard in Austria. In: 10th European Conference on Earthquake Engineering G. Duma, (ed.), Balkema, Rotterdam, 63-68, 1995.

Lenhardt, W., Svancera, J., Melichar, P., Pazdirkova, J., Havir, J., and Sykorova, Z., Seismic activity of the Alpine-Carpathian-Bohemian Massif region with regard to geological and potential field data. Geol. Carpath., 58, 397-412, 2007.

Liu, M., Stein, S., and Wang, H., 2000 years of migrating earthquakes in North China: How earthquakes in midcontinents differ from those at plate boundaries, Lithosphere 3, 128-132, doi:10.1130/L129.1, 2011.

Linzer, H. G., Decker, K., Peresson, H., Dell'Mour, R., and Frisch, W., Balancing lateral orogenic float of the Eastern Alps. Tectonophysics, 354, 211-237, doi:10.1016/S0040-1951(02)00337-2, 2002.

Formatted: German (Germany)

Formatted: German (Austria)

Formatted: highwire-cite-metadata-doi

Formatted: Footer

Linzer, H. G., Moser, F., Nemes, F., Ratschbacher, L., and Sperner, B. Build-up and dismembering of the eastern Northern Calcareous Alps. Tectonophysics, 272, 97-124, doi:10.1016/S0040-1951(02)00337-2, 1997.

McCalpin, J., Paleoseismology, 2nd ed., International Geophysics Series, 95, 613 p., 2008.

Meghraoui, M., Delouis, B., Ferry, M., Giardini, D., Huggenberger, P., Spottke, I., and Granet, M., Active Normal Faulting in the Upper Rhine Graben and Paleoseismic Identification of the 1356 Basel Earthquake. Science, 293, 2070-2073, 2001.

~~Murray, A.S., Wintle, A.S., Luminescence dating of Quartz using an improved single aliquot regenerative dose protocol, Radiat. Meas., 32, 57–73, 2000.~~

Passone, L. and Mai, M., Effects of listricity on near field ground motions: the kinematic case, Geophysical Research Abstracts, 18, EGU2016-7231, 2016.

Peters, G., Buchmann, T., Connolly, P., van Balen, R.T., Wenzel, F., and Cloetingh, S., Interplay between tectonic, fluvial and erosional processes along the Western Border Fault of the northern Upper Rhine Graben, Germany. Tectonophysics, 406, 39-66, 2005.

Preusser, F., Degering, D., Fuchs, M., Hilgers, A., Kadereit, A., Klasen, N., Krbetschek, M., Richter, D., and Spencer, J., Luminescence dating: basics, methods and applications, Eiszeitalter Gegenwart Quat. Sci. J., 57, 95–149, 2008

Procházková, D. and Šimunek, P., Fundamental data for determining seismic hazard for localities in Central Europe. Gradus, Praha, Czech Republic, 1998.

Ratschbacher, L., Frisch, W., Linzer, H.-G., and O. Merle, Lateral extrusion in the eastern Alps, Part 2: Structural analysis, Tectonics, 10(2), 257–271, doi:10.1029/90TC02623, 1991.

Rhodes, E., Optically stimulated luminescence dating of sediments over the past 200,000 years, Annu. Rev. Earth Planet. Sci., 39, 461–488, 2011.

Royden, L.H., The Vienna Basin: A thin skinned pull apart basin. In: Strike-slip deformation, basin formation, and sedimentation (Biddle, K.T. and Christie-Blick, N., Eds.). Tulsa, Oklahoma, USA, SEMP Special publications, 37, 319-340, 1985.

Salcher, B. C., Meurers, B., Smit, J., Decker, K., Hölzel, M., and Wagreich, M., Strike-slip tectonics and Quaternary basin formation along the Vienna Basin fault system inferred from Bouguer gravity derivatives. Tectonics, 31, doi: 10.1029/2011TC002979, 2012.

Šefara, J., Kováč, M., Plašienka, D., and Šujan, M., Seismogenic zones in the Eastern Alpine-Western Carpathian-Pannonian junction area. Geol. Carpath., 49, 247-260, 1998.

Spahic, D., Grasemann, B., and Exner, U., Identifying fault segments from 3D fault grad analysis (Vienna Basin, Austria). J. Struc. Geol., 55, 182-195, 2013.

Formatted: article-header__meta-info-data

Formatted: Footer

Štěpančíková, P., Hók, P., Nývlt, D., Dohnal, J., Sýkorová, I., and Stemberk, J., Active tectonic research using trenching technique on the south-eastern section of the Sudetic Marginal Fault (NE Bohemian Massif, central Europe). Tectonophysics, 485, 269-282, 2010.

Tóth, L., Györi, E., Mónus, P., and Zsiros, T., Seismic hazard in the Pannonian region. In: The Adria Microplate: GPS Geodesy, Tectonics and Hazards (Pinter, N., Grenerczy, G., Weber, J., Stein, S. and Medak, D., Eds.) Springer Verlag, Dordrecht, the Netherlands, 369-384, 2006.

van den Berg, M., Vanneste, K., Dost, B., Lokhorst, A, van Eijk, M, and Verbeeck, K., Paleoseismic investigations along the Peel Boundary Fault: geological setting, site selection and trenching results. Neth. J. Geosci., 81, 39-60, 2002.

Vanneste, K., Camelbeeck, T., and Verbeeck, K., A model of composite seismic sources for the Lower Rhine Graben, Northwest Europe. Bull. Seismol. Soc. Am., 103, 984-1007, 2013.

Vanneste, K. and Verbeeck, K., Paleoseismological analysis of the Rurrand fault near Jülich, Roer Valley graben, Germany: Coseismic or aseismic faulting history? Neth. J. Geosci., 80, 155-169, 2001.

Wallace, R. E., Grouping and migration of surface faulting and variation in slip rates on faults in the Great Basin province, Bull. Seismol. Soc. Am., 77, 868–877, 1987,

Wallinga, J., Murray, A.S., Wintle, A.G., The single-aliquot regenerative-dose (SAR) protocol applied to coarse-grain feldspar. Radiat. Meas., 32, 529-533, 2000.

Weissl, M., Hintersberger, E., Lomax, J., Lüthgens, C., and Decker, K., Active tectonics and geomorphology of the Gaenserndorf Terrace in the Central Vienna Basin (Austria). Quatern. Int., ~~in print, doi: 10.1016/j.quaint.2016.11.022~~451, 209-222, 2017.

Wessely, G., Wiener Becken, In: Wessely, G. (Ed.), Geologie der österreichischen Bundesländer: Niederösterreich, Geologische Bundesanstalt, Vienna, 189–226, 2006.

Wells, D.L. and Coppersmith, K.J., New Empirical Relationships among Magnitude, Rupture Length, Rupture Width, Rupture Area, and Surface Displacement. Bull. Seismol. Soc. Am., 84, 974-1002, 1994.

Wintle, A.G., Luminescence dating: where it has been and where it is going, Boreas, 37, 471–482, 2008.

Formatted: German (Austria)

Formatted: German (Austria)

Formatted: Font: Not Bold, Font color: Auto

Formatted: Footer

Tables

Sample	Location	Depth (m)	Moisture (%)	238U (ppm)	232Th (ppm)	K (%)	De (Gy)	D_0 (Gy/ka)	Age (ka)
AIP 25*	WAG cover	1.0	12 ± 7	2.58 ± 0.04	8.42 ± 0.23	1.12 ± 0.02	44.7 ± 2.3	2.78 ± 0.26	16.1 ± 1.7
AIP 26*	WAG cover	0.5	12 ± 7	2.35 ± 0.04	7.62 ± 0.21	1.01 ± 0.01	39.0 ± 1.4	2.01 ± 0.16	15.1 ± 1.5
AIP 38*	SDF1 fw	3.7	10 ± 7	0.82 ± 0.02	3.54 ± 0.11	1.17 ± 0.02	543.1 ± 33.7	2.13 ± 0.20	255 ± 29
AIP 39*	SDF1 hw	3.6	10 ± 7	1.78 ± 0.03	7.56 ± 0.21	1.18 ± 0.02	273.5 ± 20.2	2.64 ± 0.25	104 ± 12
AIP 40*	SDF1 hw	3.3	10 ± 7	1.84 ± 0.03	7.64 ± 0.21	1.24 ± 0.02	154.0 ± 5.5	2.72 ± 0.25	56.6 ± 5.7
AIP41*	SDF1 hw	2.6	10 ± 7	2.69 ± 0.04	10.46 ± 0.28	1.61 ± 0.02	168.7 ± 5.9	3.45 ± 0.32	48.9 ± 4.8
AIP44*	SDF1 hw	1.9	10 ± 7	1.49 ± 0.03	5.92 ± 0.17	0.91 ± 0.01	36.7 ± 2.1	2.26 ± 0.22	16.3 ± 1.8
AIP 46*	SDF1 hw	1.2	10 ± 7	2.39 ± 0.04	9.12 ± 0.25	1.44 ± 0.02	43.6 ± 1.6	2.01 ± 0.16	13.8 ± 1.4
AIP 93	SDF3 hw	4.1	12 ± 7	1.64 ± 0.03	8.06 ± 0.22	1.25 ± 0.02	419.2 ± 39.4	3.17 ± 0.30	158 ± 21
AIP 95	SDF3 hw	3.1	12 ± 7	1.87 ± 0.03	9.41 ± 0.26	0.97 ± 0.02	317.4 ± 29.1	2.58 ± 0.24	123 ± 16
AIP 96	SDF3 hw	2.6	12 ± 7	2.22 ± 0.04	8.96 ± 0.24	1.26 ± 0.02	292.0 ± 13.5	2.62 ± 0.25	111 ± 12
AIP97	SDF3 hw	2.1	12 ± 7	2.22 ± 0.04	8.96 ± 0.24	1.26 ± 0.02	205.1 ± 13.3	2.90 ± 0.26	70.8 ± 8.0
AIP98	SDF3 hw	1.8	12 ± 7	2.19 ± 0.04	8.28 ± 0.25	1.19 ± 0.02	91.6 ± 7.5	2.78 ± 0.25	32.9 ± 4.1
AIP102	SDF3 hw	0.3	15 ± 7	3.01 ± 0.04	12.14 ± 0.33	1.30 ± 0.02	15.7 ± 0.9	3.29 ± 0.30	4.8 ± 0.5
AIP103	SDF3 fw	1.4	10 ± 7	0.57 ± 0.01	1.79 ± 0.06	1.04 ± 0.02	384.6 ± 59.7	1.88 ± 0.18	205 ± 37
AIP 114	SDF3 fw	0.65	10 ± 7	0.57 ± 0.01	1.79 ± 0.06	1.04 ± 0.02	468.3 ± 43.4	1.81 ± 0.17	259 ± 35

Event #	Evidence	Thickness of colluvial wedge @ NE wall	Thickness of colluvial wedge @ SW wall	Displacement
C2	cw	-	-	-

Table 1: Type of evidence and inferred displacement for the paleoearthquakes A1 to A5 (trench SDF1), B1 to B5 (SDF3), and C1 toC2 (WAG). Also listed are the thicknesses of colluvial wedges observed in the NW and SE trench walls used for estimating displacement. Table 1 Evidence: displacement of correlated layers (displ.), occurrence of colluvial wedges (cw), and sediment-filled tension cracks below the colluvial wedges (tc). **Displacement is taken as twice the thickness of the colluvial wedge.**

Sample	Location	Method	De (Gy)	D_0 (Gy/ka)	Depth (m)	Water (%)	Age (ka)
AIP25	WAG cover	IRSL	44.7 ± 2.3	2.78 ± 0.26	1.0	12	16.1 ± 1.7
AIP26	WAG cover	IRSL	39.0 ± 1.4	2.01 ± 0.16	0.5	12	15.1 ± 1.5
AIP38	SDF1 fw	IRSL	543.1 ± 33.7	2.13 ± 0.20	3.7	10	255 ± 29
AIP39	SDF1 hw	IRSL	273.5 ± 20.2	2.64 ± 0.25	3.6	10	104 ± 12
AIP40	SDF1 hw	IRSL	154.0 ± 5.5	2.72 ± 0.25	3.3	10	56.6 ± 5.7
AIP41	SDF1 hw	IRSL	168.7 ± 5.9	3.45 ± 0.32	2.6	10	48.9 ± 4.8
AIP44	SDF1 hw	IRSL	36.7 ± 2.1	2.26 ± 0.22	1.9	10	16.3 ± 1.8
AIP46	SDF1 hw	IRSL	43.6 ± 1.6	2.01 ± 0.16	1.2	10	13.8 ± 1.4
AIP93	SDF3 hw	IRSL	419.2 ± 39.4	3.17 ± 0.30	4.1	12	158 ± 21
AIP95	SDF3 hw	IRSL	317.4 ± 29.1	2.58 ± 0.24	3.1	12	123 ± 16
AIP97	SDF3 hw	IRSL	205.1 ± 13.3	2.90 ± 0.26	2.1	12	70.8 ± 8.0
AIP98	SDF3 hw	IRSL	91.6 ± 7.5	2.78 ± 0.25	1.8	12	32.9 ± 4.1
AIP102	SDF3 hw	IRSL	15.7 ± 0.9	3.29 ± 0.30	0.3	15	4.8 ± 0.5
AIP103	SDF3 fw	IRSL	384.6 ± 59.7	1.88 ± 0.18	1.4	10	205 ± 37
AIP114	SDF3 fw	IRSL	468.3 ± 43.4	1.81 ± 0.17	0.65	10	259 ± 35

Table 2: Infrared stimulated Luminescence (IRSL) and optically stimulated luminescence (OSL) dating results from the trenches SDF1, SDF3, and WAG at the Markgrafneusiedl Fault (MF). * refer to samples already published by Weissl et al. (2017). Location: refers to either of the trenches (SDF1, SDF3, WAG) and the location in respect to the MF, where hw = hanging wall and fw = footwall. N: number of used aliquots. De (Gy): equivalent dose in Gray (Gy), D_0 (Gy/ka): dose rate in Gray values (per 1,000 years); Depth (m): depth of the sampling location in meters below present-day surface.

Formatted: Font: Not Bold, Font color: Auto

Formatted

Formatted: Caption, Right: 0 cm, Line spacing: single

Formatted: Footer

Event #	Evidence Correlation	Ante quem Event older than (age / sample location)Thickness of colluvial wedge @ NE wall	Postquem Event younger than (age / sample location)Thickness of colluvial wedge @ SW wall	Displacement	Occurrence time
A1	displ	-	-	0.15 - 0.25 m	15.1 ± 2.2 ka
E1A2	cw, tc A1 = B1 = C1	0.95 m	0.75 m	13.8 ± 1.4 ka (SDF1), 4.8 ± 0.5 ka (SDF3)1.50 - 1.90 m	32.9 ± 27.5 ± 13.4.1 ka (SDF3), 16.3 ± 1.8 ka (SDF1), 15.1 ± 1.5 ka (WAG)
A3	cw, tc	0.45 m	0.40 m	0.80 - 0.90 m	38.4 ± 14.4 ka
E2A4	cw, tc A2 = B2 = C2	0.75 m	0.72 m	1.40 - 1.50 m32.9 ± 4.1 ka (SDF3), 16.1 ± 1.7 ka (SDF1)	7074.0 ± 21.8 ± 8.0 ka (SDF3), 48.9 ± 4.8 ka (SDF1)
E3A5	A3, ?= B3?cw	0.25 m	0.40 m	0.50 - 0.80 m	3290.1 ± 22.9 ± 4.1 ka (SDF3), 16.1 ± 1.7 ka (SDF1) 70.8 ± 8.0 ka (SDF3), 48.9 ± 4.8 ka (SDF1)
B1	displ	-	-	0.10 - 0.15 m	18.3 ± 13.5 ka
E4B2	A4, ?= B3?cw		0.8	0.8/1.6 m	56.6 ± 5.7 ka (SDF1) 3244.9 ± 17.4.1 ka (SDF3), 104 ± 12 ka (SDF1), 70.8 ± 8.0 ka (SDF3)
E5B3	?A4 =? B4tc	-	-	-	111 ± 1257.7 ± 18.5 ka (SDF3), 56.6 ± 5.7 ka (SDF1) 123 ± 16 ka (SDF3), 104 ± 12 ka (SDF1)
B4	cw	-	-	-	115 ± 14 ka
E6B5	A5 ?= B4?cw	111 ± 12 ka (SDF3), 56.6 ± 5.7 ka (SDF1)-	-	-	123 ± 1614 ka (SDF3), 104 ± 12 ka (SDF1)
C1	displ	-	-	0.17 - 0.20 m	<15.1 ± 1.5 ka
E7C2	?A5 = B5?cw	-	-	-	111 ± 12 ka (SDF3), 123 ± 16 ka (SDF3), 104 ± 12 ka (SDF1)

					56.6 ± 5>16.1 ± 1.7 ka (SDF1)	
	E8	B5	111 ± 12 ka (SDF3)	123 ± 16 ka (SDF3)		

Table 2: Type of evidence, inferred displacement for the paleoearthquakes A1 to A5 (trench SDF1), B1 to B5 (SDF3), and C1 to C2 (WAG) and possible occurrence time. Colluvial wedge thickness observed on NE and SW trench walls used for estimating displacement. Displacement is taken as twice the colluvial wedge thickness. Evidence: displacement of correlated layers (displ.), occurrence of colluvial wedges (cw), and sediment-filled tension cracks below the colluvial wedges (tc). 3:Occurrence times (mean ± 2σ) are calculated with OxCal using chronological constraints from respective trenches.

Event #	Correlation	*Antequem* Event older than (age / sample location)	*Postquem* Event younger than (age / sample location)	*Magnitude* $M(d_{max})$ $M(d_{ave})$	*Occurrence interval* OxCal result (mean ± 1σ)
E1	A1 = B1 = C1	**13.8 ± 1.4 ka (SDF1),** 4.8 ± 0.5 ka (SDF3)	32.9 ± 4.1 ka (SDF3), 16.3 ± 1.8 ka (SDF1), **15.1 ± 1.5 ka (WAG)**	6.2 ± 0.5 *6.3 ± 0.6*	14.2 ± 0.8 ka (SM1/2)
E2	A2 = B2 = C2	**32.9 ± 4.1 ka (SDF3),** 16.1 ± 1.7 ka (SDF1)	70.8 ± 8.0 ka (SDF3), **48.9 ± 4.8 ka (SDF1)**	6.8 ± 0.4	37.1 ± 4.9 ka (SM1/2)
E3	A3, ?= B3?	**32.9 ± 4.1 ka (SDF3),** 16.1 ± 1.7 ka (SDF1)	70.8 ± 8.0 ka (SDF3), **48.9 ± 4.8 ka (SDF1)**	6.6 ± 0.4	43.4 ± 4.9 ka (SM1/2)
E4a	A4, ?= B3?	**56.6 ± 5.7 ka (SDF1)** 32.9 ± 4.1 ka (SDF3),	104 ± 12 ka (SDF1), **70.8 ± 8.0 ka (SDF3)**	6.8 ± 0.5	64.9 ± 5.6 ka (SM1)
E4b	?A4 =? B4	**111 ± 12 ka (SDF3),** 56.6 ± 5.7 ka (SDF1)	123 ± 16 ka (SDF3), **104 ± 12 ka (SDF1)**	6.8 ± 0.5	106 ± 3 ka (SM2)
E5a	A5 ?= B4?	**111 ± 12 ka (SDF3),** 56.6 ± 5.7 ka (SDF1)	123 ± 16 ka (SDF3), **104 ± 12 ka (SDF1)**	6.5 ± 0.4	107 ± 4 ka (SM1)
E5b	?A5 = B5?	**111 ± 12 ka (SDF3),** 56.6 ± 5.7 ka (SDF1)	123 ± 16 ka (SDF3), **104 ± 12 ka (SDF1)**	6.5 ± 0.4	109 ± 3 ka (SM2)
E6a	B5	**111 ± 12 ka (SDF3)**	**123 ± 16 ka (SDF3)**	-	120 ± 7 ka (SM1)

Table 1: Overview of common IRSL constraint for characteristics of each possible earthquake derived from all different sites. Agescommon. IRSL constraints in bold mark the upper and lower limit for each occurrence time. Occurrence times are calculated with OxCal (see Figure 11) using stratigraphic constraints from all sites. SM1 and SM2 refer to slip model 1 and 2, respectively. For details about correlation between the trenches, see sect. 5.

Formatted: Centered, Indent: Left: 0 cm, Right: 0 cm, Line spacing: single, Keep with next

Formatted ...

Formatted ...

Formatted: Font color: Auto

Formatted: Caption, Indent: Left: 0 cm, Right: 0 cm, Line spacing: single

Formatted ...

Formatted: Footer

Formatted: Footer

Figure captions

Figure 1: (A) Active faults (black solid and dashed lines), seismicity (black circles) and Quaternary basins (light grey areas) within the Vienna Basin (Austria) plotted on a shaded DEM. Seismicity is based on the ACORN catalogue (2004). The borders of the Austrian capital, Vienna, is outlined by a dashed white line. Modified after Beidinger and Decker (2011). White box shows the location of the close up inVBTF = Vienna Basin Transfer Fault. Important splay normal faults of the VBTF: ABF = Aderklaa-Bockfliess Fault, BNF = Bisamberg-Nussdorf Fault, LF = Leopoldsdorf Fault, MF = Markgrafneusiedl Fault. White box shows the location of Figure 3A, white line the position of the cross section of Figure 2; (B) Major earthquakes from historical, instrumental and paleoseismological data in intra-plate Central Europe. Historical and instrumental seismicity is based on the CENEC Catalogue by Grünthal et al., 2009. PaleositesPaleoseismological study sites are compiled from Camelbeeck and Meghraoui, 1998; Camelbeeck et al., 2000; 2007; Meghraoui et al., 2001; Vanneste and Verbeeck, 2001; van den Berg et al., 2002, Peters, et al., 2005; Štěpančíková et al., 2010. Labels indicate the magnitudes of the largest paleoearthquakes observed at the respective site. Black box shows area of the close up in (A). MF= Markgrafneusiedl Fault; VBTFVBFS = Vienna Basin Fault System.

Figure 2: Cross section through the Vienna Basin at its central part based on reflection seismic and deep boreholes indicating the common detachment of the Alpine floor thrust, which links the splay normal faults, such as the Markgrafneusiedl Fault (MF), to the Vienna Basin Transfer Fault (VBTF). Redrawn from Hölzel et al. (2010).The generalized detachment corresponds to the Alpine-Carpathian floor thrust, which is reactivated by normal faulting.

Figure 3: Overview of the Markgrafneusiedl Fault (MF.). (A) DEM showing the Pleistocene terraces north of the River Danube dissected by faults creating fault scarps (fs). GDT = Gaenserndorf terrace, SHT = Schlosshof terrace. Dashed line: trace of the topographic profile in B, solid line: trace of the seismic line in C., white circle: locations of the villages Markgrafneusiedl (MGNS) and Gaenserndorf (GD). (B) Topographic profile (black) and cross-section indicating the base of Quaternary sediments (grey) across the MF. Note the thickness of Quaternary growth strata in the fault-delimited basin above the MF. Vertical exaggeration: 8.6 (C) seismic section across the same area showing offset along the Markgrafneusiedl Fault (MF) and the flower structure at the Vienna Basin Transfer Fault (right).VBTF). Vertical exaggeration at 2s TWT: 4.5. See text for details.

Figure 4: Photo mosaic Trench locations of SDF1 and interpretationSDF3. (A) Locations of trenches SDF1 and SDF3 relative to the margin of the Gaenserndorf terrace (light grey in DEM) and the Markgrafneusiedl Fault (MF). Depressions normal to the MF are currently dry valleys resulting from Pleistocene drainage of the terrace. Digital elevation model with a resolution of 10x10 m. (B) View of the fault scarp south of the forested area where the trenches are located, looking towards the N. (C) Trench location of SDF3, looking NW towards the footwall. Trench runs parallel to the trees. (D) Trench SDF 3 during excavation, looking SE towards the hanging wall. Note the difference in elevation between standing position and trees in the back. (E) Trench location of SDF1,

Formatted: Caption, Line spacing: 1,5 lines

Formatted: Caption, Line spacing: 1,5 lines

Formatted: Keep with next

Formatted: Footer

looking NW towards the footwall. (F) Trench SDF1 during excavation, looking SE towards the hanging wall. Note the difference in elevation between standing position and crop in the back.

Figure 5: Trench log of the SW-facing wall of the trench SDF1 across the Markgrafneusiedl Fault (for location see Figure 2). ColluvialFigures 3A and 4). Stratigraphic units are marked with U1-U11 from the oldest to the youngest unit, colluvial wedges and underlying tension cracks related to earthquakes A2-A5 are numbered. The displacement related to A1 is marked. as W2-W5 and T2-T5. Numbers indicate the age and the location of IRSL and OSL samples. See text for further explanation. See supplementary for high-resolution photomosaique.

Figure 56: Details from the SW-facing wall of the trench SDF1. (A) Evidence for earthquake A1 from the displacement of a marker horizon (white arrows), which is correlated across the fault (red arrows). (b) Evidence for earthquake A2 from a colluvial wedge composed of sandy gravel overlying a tension gash filled with the same material (. Top and base of the wedge are marked by white and yellow arrows)., respectively. To the right the wedge abuts against fault 1 (red arrows). (C) Colluvial wedge associated with earthquake A3 (white arrows) overlying a tension gash adjacent to fault 2. (yellow and orange arrows: top and base of the wedge/tension gash; red arrows: fault). Several deformation bands that branch from fault 2 and formed during a later earthquake cut the wedge. It overlies wedge 4, which equally contains reddish redeposited soil. Wedge 4 shows an erosional contact to grey high-stage flood sediments (around box E). (D) Deformation bands offsetting laminated fluvial sand (red arrows) above wedge 2. The deformation bands are correlated to the event horizon of E1 (detail of picture B). (E) Detail of (C). Erosional contact of wedge 4 to flood sediments. Armoured mudballs (arrow) derive from the eroded colluvium.

Figure 6: Photo mosaic and interpretation7: Trench log of the SW-facing wall of the trench SDF3 across the Markgrafneusiedl Fault (for location see Figure 2Figures 3A and 4). Colluvial wedges and underlying tension cracks related to earthquakes B2-B5 are numbered. The displacement related to B1 is marked. Numbers indicate the age and the location of IRSL and OSL samples. Additional information is provided in theSee text. for further explanation. See supplementary for high-resolution photomosaique.

Figure 78: Details from the SWW-facing wall of the trench SDF3. (A) Wedge associated with earthquake B2 (top: white arrows; base: yellow arrows; see text for discussion) overlying wide fault (red arrows). Thean upward widening fault is(red arrows), recognized from pebbles, which are oriented parallel to the fault. The top of the wedge (white arrows) is offset by a narrow deformation band that emerges from the fault below the wedge (purple arrows). Offset occurred during B1. (B, C) Laminated flood sediments (clay, silt and fine sand) underlying colluvium of wedge B2. Pebbles sunken into the soft sediment (B) and flame structures protruding into the overlying gravel (C) are indicative for liquefaction.

Figure 89: (A) Trench WAG, photo mosaic of the SWW-facing trench wall. Red arrows denote locations of faults, white. Yellow arrows point to offset contact between colluvium and overlying loess. Orange arrows denote location of the faulted marker layer depicted in Figure 10. Boxes refer to details shown in Figure 910 B and C.

Figure ~~9~~10: (A) Trench WAG looking ~~E~~NW toward the footwall of the MF (fault trace denoted by red arrows). Note offset of bright layer of loess (white arrows) corresponding to C1. CW denotes the colluvial wedge related to earthquake C2. (b) Detail of the SW-facing trench wall. Red arrows denote locations of faults, ~~white~~orange arrows point to the offset contact between grey and brown silt and clay. Box shows location of details shown in D. (C) Offset of the top of the colluvial wedge associated with earthquake C2 (~~white~~yellow arrows). (D, E) Fractured and sheared pebbles indicating normal displacement parallel to the slip of the MF. Note that fractures in pebbles are filled with sandy matrix excluding fracture formation during construction work.

Figure ~~10~~11: Comparison of age constraints from all trench sites SDF1, SDF3, and WAG and possible occurrence times of the observed earthquakes for the two possible ~~correlations.~~slip models. The central panel shows the age constraints and earthquake occurrence times for each site separately. For the WAG site, only maximum constraint for C1 and minimum constraint for C2 are available. The upper and lower panels show the resultant earthquake occurrence times considering the combined chrono-stratigraphic constraints from all sites together for slip models 1 and 2, respectively. For details about correlation see sect. 5. Calculations carried out using OxCal v4.3.2 (Bronk Ramsey, 1995, 2001).

Figure ~~11~~12: Recurrence intervals for slip model 1 (upper panel) and slip model 2 (lower panel), respectively.

Figure 13: Comparison of surface slip rates for the Markgrafneusiedl Fault (MF) from geomorphic constraints and from trench results. On the left the constraints for ~~event line~~slip model 1 are plotted, on the right, those for ~~event line~~slip model 2 are shown.

Figure ~~12:~~14: Geometry and fault area of the Markgrafneusiedl Fault (MF). Also shown are the Vienna Basin Transfer Fault (VBTF) and other active normal splay faults branching from the VBTF. ABF: ~~Adreklaa~~Aderklaa-Bockfliess fault system; BNF: Bisamberg-Nussdorf fault; LF: Leopoldsdorf fault; SF: Seyring fault (redrawn from Decker et al., 2015). Broken grey line marks the city limits of Vienna.

Formatted: Keep with next

Formatted: Caption, Line spacing: 1,5 lines

Formatted: Caption, Line spacing: 1,5 lines

Formatted: Footer

Formatted: Font: 9 pt

Formatted: Heading 1

Formatted: Footer